remote sensing

MDPI

Review

Overview of the Application of Remote Sensing in Effective Monitoring of Water Quality Parameters

Godson Ebenezer Adjovu, Haroon Stephen, David James and Sajjad Ahmad *

Department of Civil and Environmental Engineering and Construction, University of Nevada Las Vegas, Las Vegas, NV 89154, USA
* Correspondence: sajjad.ahmad@unlv.edu; Tel.: +1-702-895-5456

Abstract: This study provides an overview of the techniques, shortcomings, and strengths of remote sensing (RS) applications in the effective retrieval and monitoring of water quality parameters (WQPs) such as chlorophyll-a concentration, turbidity, total suspended solids, colored dissolved organic matter, total dissolved solids among others. To be effectively retrieved by RS, these WQPs are categorized as optically active or inactive based on their influence on the optical characteristics measured by RS sensors. RS applications offer the opportunity for decisionmakers to quantify and monitor WQPs on a spatiotemporal scale effectively. The use of RS for water quality monitoring has been explored in many studies using empirical, analytical, semi-empirical, and machine-learning algorithms. RS spectral signatures have been applied for the estimation of WQPs using two categories of RS, namely, microwave and optical sensors. Optical RS, which has been heavily applied in the estimation of WQPs, is further grouped as spaceborne and airborne sensors based on the platform they are on board. The choice of a particular sensor to be used in any RS application depends on various factors including cost, and spatial, spectral, and temporal resolutions of the images. Some of the known satellite sensors used in the literature and reviewed in this paper include the Multispectral Instrument aboard Sentinel-2A/B, Moderate Resolution Imaging Spectroradiometer, Landsat Thematic Mapper, Enhanced Thematic Mapper, and Operational Land Imager.

Keywords: airborne sensors; machine learning; monitoring; remote sensing; resolution; spectral signatures; spaceborne sensors; water quality parameters

Citation: Adjovu, G.E.; Stephen, H.; James, D.; Ahmad, S. Overview of the Application of Remote Sensing in Effective Monitoring of Water Quality Parameters. *Remote Sens.* **2023**, *15*, 1938. https://doi.org/10.3390/rs15071938

Academic Editor: Gabriel Senay

Received: 11 February 2023
Revised: 26 March 2023
Accepted: 1 April 2023
Published: 4 April 2023

1. Introduction

Water quality parameters (WQPs) have traditionally been analyzed and monitored through in situ sampling and laboratory testing; however, these approaches are expensive, labor-intensive, time-consuming, and not suitable for large-scale analysis. Sample collections are therefore limited over spatial and temporal scales [1–5]. The use of these conventional methods in water quality monitoring has been taxing due to limited resources in terms of capital and labor available particularly in developing countries. Conventional methods have limited capability to capture the horizontal heterogeneity in the water ecosystem on a large scale and extent. Monitoring, management, and forecasting of the entire water bodies may be inaccessible due to the topographic terrain of the water body. Furthermore, the accuracy and precision of sampled in situ data can be questionable owing to both errors that may arise from field sampling and laboratory analysis [6–9]. These limitations have put constraints on efforts to monitor the ecological suitability of water bodies over the past decades. Remote sensing (RS) application alternatives have been used in water quality monitoring at local, regional, and global scales in the last six decades and can overcome the limitations associated with conventional methods [10–12].

The paper provides a compilation of efforts utilized in the monitoring of WQPs using RS, satellite sensors, and wave bands as were available through 2022 for several WQPs. This review also evaluates the strengths and limitations that could lead to errors, including

image processing errors, pixel resampling problems, and atmospheric interference of the sensors and platforms, which are necessary for continued research in the field of RS in water quality monitoring.

RS applications for water quality monitoring offer synoptic spatial and temporal coverage of the water body that is unattainable by conventional methods, making it ideal and suited for the cost-effective assessment of water quality [8,13]. Most of the satellite images are made available at no cost to users [3]. RS applications, unlike in situ field measurement, allow for analyses of WQPs on a large scale, and hence, are not limited to a single location in space and time. These applications aid to fill the global gap in the spatiotemporal data. They also provide present-time and comparable accurate results at a very fast pace [2,14–18]. Water resources researchers, decision, and policymakers can rely on remotely sensed data to reinforce their abilities in the effective monitoring of the fast-depleting water resources [19]. RS coupled with strategic in situ measurement and monitoring is a useful tool in aiding to predict, mitigate, and possibly prevent future water quality issues [20].

RS sensors capture spectral signatures of water constituents, which makes them an effective tool for the estimation of different WQPs including TSS and chlorophyll-a concentration [1]. Several studies have been carried out that have utilized RS applications in the qualitative and quantitative determinations of WQPs. Qualitative determinations include the identification of the presence, absence, or approximation of WQPs. When RS is combined with calibration curves from ground truth observations, quantitative estimates can be obtained, which are of much greater value to water scientists, engineers, planners, regulators, and policymakers.

Different RS sensors have been reportedly used in the estimation of WQPs, including Landsat 5, 7, and 8 Operational Land Imager (OLI) sensors, Advanced Spaceborne Thermal Emission and Reflection Radiometer (ASTER) images, Sentinel-2A/B Multispectral Instruments (MSI), Pleiades-1A, Moderate Resolution Imaging Spectroradiometer (MODIS), and Medium-Resolution Imaging Spectrometer (MERIS); these sensors have been used extensively to effectively quantify various parameters, including but not limited to, chlorophyll-a concentration, turbidity, TSS, total phosphate, COD concentration, algae content, total dissolved organic matter, colored dissolved organic matter (CDOM), dissolved organic carbon (DOC), Secchi disk depth (SDD), pH, and total dissolved solids (TDS), in inland and coastal water bodies [8,15,17,21–32]. WQPs such as TSS and CDOM have been effectively determined using RS techniques because they are spectrally active in the visible and IR portions of the electromagnetic spectrum.

RS has been utilized as an efficient tool for supporting the implementation of the European Union Water Framework Directive (EU WFD) as it provides needed tools for the derivation of WQPs including CDOM, total suspended matter (TSM), chlorophyll-a, the spectral attenuation coefficient, and phycocyanin [33,34]. Methods used to retrieve WQPs are dependent on the optical properties of the inland water bodies since the measurement parameters are mostly physical, chemical, or biological [1,35]. WQPs are categorized as either optically active or weak variables. Optically active parameters are constituents of the water that interact with light and subsequently change the energy spectrum of reflected solar radiation from water bodies. These parameters can be measured with RS. Parameters such as total suspended solids (TSS), suspended materials/solids (SM), chlorophyll-a, and turbidity constitute optically active parameters, while total nitrogen (TN), ammonia nitrogen (NH3-N), pH, dissolved oxygen, micro-pollutants, and dissolved phosphorus (DP) are either optically weak with a low signal/noise ratio or are optically inactive in the visible and near IR. These weak parameters are estimated through inference by association with active optical parameters, and proxy assimilation.

Optically active parameters are, however, complex if a reflected signal contains information from more than one constituent and is spatially and temporally variable. The retrieval of these parameters is therefore applicable using specific sensors and in particular environments [1,10,16,36,37].

One of the important parameters for reflecting water quality is water color. The water color is determined by the absorption and scattering of water components due to the interactions between sunlight and various materials in the water. The interaction between the concentration of optically active substances in the water and the color of the water makes it a crucial criterion for affecting water quality [1]. For example, dissolved organic matter absorbs light in both the visible and ultraviolet range of the electromagnetic spectrum, thereby affecting the volume of reflectance at a shorter wavelength [38].

2. Water Quality Monitoring

This section provides an overview of the literature on the efforts carried out on water degradation and WQPs.

2.1. Water Resources Degradation

Water resources cover about 75% of the earth's surface, However, only 3% is portable. Approximately, 25% of the world's population does not have access to a satisfactory quantity and or quality of freshwater [39]. Water bodies are crucial to the existence of humans, aquatic life, and the whole ecosystem. Water bodies including inland waters are the main source of water for drinking, power generation, industrial cooling, supporting biodiversity, ecosystem services, recreation, transportation routes, waste disposal, agriculture production, energy production, regional planning, and fish farming [11,18,40–45]. Inland water bodies are at the receiving end of the effect of climate change, development, urbanization, and contamination caused by rapid and uncontrolled environmental changes including nutrient pollution, drought, and changes in land use and land cover, which results in negative impacts such as the proliferation of toxic blue-green algae, extreme turbidity, accelerated eutrophication among others, which impacts the sustainability of the water resources [46–49]. Eutrophication in water bodies is a condition that leads to significant changes in the algal nutrient loads, which then leads to an imbalance in the water ecosystem with a bloom of algal and intense oxygen consumption at the bottom of the lakes posing a threat to the water ecosystem. This situation has the potential to alter the pristine ecological conditions of water bodies [12,42,50]. Anthropogenic activities such as irrigation, the use of fertilizers, grazing, indiscriminate discharge of untreated sewage from wastewater treatments, and economic development around watersheds, particularly in industrial areas, are continually causing the impairment and degradation of freshwater systems such as lakes and rivers [17,45,51–54]. The degradation of water bodies including river catchments is one of the important issues of environmental concern affecting the quality of water in tropical countries [55]. Studies have shown that rivers and streams flowing through the Great Plains of Central North America are now endangered and deteriorated and are no longer a sustainer of biodiversity [56]. In some watersheds, the deterioration of water bodies continues to worsen due to urbanization and climate change.

Climate change is said to be a worsening factor that poses an unending stressor on the ecological status of the water systems including lakes. The quantification of the exact role played by climate change in the ecology of the water bodies is however problematic due to the importance played by nutrients compared with slow changes occurring in the physical characteristics of the water column [50]. Climate change is known to result in corresponding changes in streamflow and the temperature of water bodies. An increase in water temperatures alters the biochemical reaction rates, causing thermal stratification in freshwater bodies. Water temperatures increase and can cause lake mixing reduction, which combined with increased oxygen consumption of biota can reduces the quality of water [57]. Climate change is also a cause of salinity intrusion, which can have a deleterious effects on agriculture production, economics, and the environment [58]. Predicting ecological and hydrological responses of water systems to climate change and their future variability is a challenge for scientists across the globe [59].

Water bodies are under intense pressure due to environmental and ecological changes caused by rapid population growth and development. A national survey on the quality of

water bodies in China reported the quality of 22.1% of the country's inland water bodies as bad. The severity of the pollution of water resources has resulted in a shortage of freshwater [1]. Water pollution is now one of the most serious issues posing a threat to the water environment, human health, and the water as a resource, which needs to be addressed with the needed urgency [5]. Pollution of water bodies was, however, appreciated as far back in human history. The Romans in 312 B.C. [60] noted that the river Tiber was too polluted to be used as drinking water. The English started considering river pollution as environmental pollution as far back as the 13th century when the laws prohibited the washing of charcoals in the River Thames in Middlesex for the fear of causing downstream pollution. By the late 19th and early 20th centuries, many of the major rivers in Europe including the Elbe, Danube, and Rhine (used as a source of drinking water by the Dutch) experienced marked pollution problems [60]. Known water quality-related issues include high organic suspended solids, high biological oxygen demand, and high ammonia levels. These led to a reduction in plant and fish species, invertebrates, and the subsequent total disappearance of fish [60].

Impairment of water resources brings about economic losses. Changes in the quality of water in rivers and lakes cause changes in the quality of recreational and commercial activities. There is a decline in boating, fishing, and swimming in these water bodies when they are impaired, which brings about significant economic losses. A study performed using biophysical modeling establishes that Virginia households may need to pay as much as USD 184 million yearly to ensure there is an improvement in the quality of their water [57].

Drinking impaired water results in waterborne diseases. Most of the reported waterborne outbreaks in North America are linked to contaminated rural drinking water systems exposed to microbial agents such as viruses, parasites, and bacteria. Water in these areas is exposed to these microbial agents due to the high agricultural activities (i.e., livestock production), and inadequate advanced treatment for human, animal, and wastewater, leading to an increase in human exposure to water contaminants [61]. An estimated 50 and 120 million cases of acute respiratory and gastrointestinal diseases associated with swimming in contaminated beach waters, respectively, are reported worldwide [62].

These issues stemming from exposure to contaminated water show the importance of managing and protecting water resources, especially concerning water quality. Protecting, restoring, and managing water resources is, however, a complex process that requires a systemic framework to deal with the issues. The process involved in water management often faces political and social contestation as opposed to regular problem-solving approaches, which are often undisputed and straightforward [63]. For example, the EU WFD, which came into action in December 2020 for all European Union member countries, ordered good ecological and chemical status in terms of pollutant levels by the year 2027 for all water bodies larger than 50 hectares in Europe. A good ecological status is described as a condition in which alterations in hydro-morphological conditions cause no more than a slight change in the abundance and composition of essential biological indicators including phytoplankton, macrophytes, and fish fauna among others [33,59].

2.2. Water Quality Parameters

Water quality is an overall indicator of the condition and general well-being of the water body, being comprised of its physical, chemical, biological, and radiological properties [1]. To protect and restore the quality of water resources, monitoring efforts and management strategies are key and need to be successful to achieve desirable results of a healthy water body in the ecosystem economy [64,65]. We cannot overemphasize the knowledge of the WQPs and their characterization in the monitoring efforts. WQPs are generally categorized as physical, chemical, and biological parameters. Physical water indicators include pH, dissolved oxygen (DO), total suspended solids (TSS), electrical conductivity (EC), salinity or total dissolved solids (TDS), nutrients such as nitrogen and phosphorus, and aesthetics (i.e., odor, color, and taints) Chemical parameters, however,

include, but are not limited to, cations such as calcium (Ca^{2+}), potassium (Na^{+}), and magnesium (Mg^{2+}) as well as anions such as nitrate (NO^{3-}), sulfate ($SO_4{}^{2-}$), and chloride (Cl^{-}); meanwhile, biological parameters include algae and bacteria such as *Escherichia coli* (*E. coli*) and total coliforms. Categorization of these parameters was performed through correlation analysis [18,66]. Other contaminants in water include volatile organic contaminants (VOCs) that are detrimental to public health and are of environmental concern due to their usage by industry-inclined countries. Some of the most organic contaminants include aromatic hydrocarbons (AHs) and chlorinated hydrocarbons (CHCs) [67]. VOCs such as tetrachloroethylene and trichloroethylene are found in groundwater while polynuclear aromatic hydrocarbons (PAHs) generated during the combustion of organic materials are found in surface water [68].

Measured WQPs are used to evaluate the degree of organic contamination of water bodies including chemical oxygen demand (COD), biochemical oxygen demand (BOD), and total organic carbon (TOC). The COD and BOD are two indicators that have been accepted as surrogate indicators of organic contaminants in water bodies [64]. TOC is made from a fraction of particulate organic carbon (POC) and dissolved organic carbon (DOC) and has been used in studies as an alternative test procedure to rapidly assess the quality of untreated and treated water. DOC in natural water is mostly composed of hydrophilic and hydrophobic [69,70]. DOC has also been considered a surrogate parameter in the quantification of dissolved organic matter (DOM) in water [71]. DOC and CDOM are key water quality indicators to examine the biogeochemical state of coastal waters [72]. Most organic matter in the water column of water systems is usually in dissolved form. DOM in water bodies such as lakes is made of a large degree of colored humic substances that find their way into water bodies from the terrestrial environments of the water bodies [73]. Quantifying CDOM in water bodies is essential to know its absolute concentration of DOM [74]. Soluble COD and DOC are parameters used in industrial or municipal plants to optimize carbon degradation processes. They are for persistent compounds in wastewater effluents that are not eliminated in the biological stage of the wastewater treatment plants (WWTPs) [75]. DOC has been linked to the spectral shape of water spectral reflectance and, in turn, used to capture mash DOC export in a study to examine the spatial features and temporal changes in DOC over a range of conditions using Landsat 8 OLI and Sentinel-2 images [76].

The detection of organic pollutants such as COD has been performed through instrumentalmethods, which include dichromate-spectrophotometry and dichromate-titration. These methods are however faced with some deficiencies including the longer amount of time needed for the determination of COD and reagents, the high cost associated with them, the need for online digestion of water samples at high pressure and temperature, and the production of secondary pollutions. Other known methods of COD measurement include hydroxyl radical oxidation-electrochemical analysis and UV absorption spectrum analysis. While UV absorption spectrum analysis does not need reagents, it has poor stability and universality owing to its absorbance and poor linear correlation with COD concentration. The hydroxyl radical oxidation-electrochemistry analysis is however able to meet the need for the rapid determination of COD at normal conditions of temperature and pressure and has no secondary pollution [77].

A known phenomenon that also affects the quality of water is lake turnover. Lake turnover has also been linked to water quality issues. Failure for lakes to turnover causes a condition known as anoxic hypolimnion, which is not suitable for the life of aquatic organisms. Water quality monitoring is therefore key to determining if there are any changes in lake mixing frequency because disturbance in the mixing capabilities of the lake reduces its quality for human and aquatic life [78]. The turnover is expected to occur twice annually in dimictic temperate lakes that freeze in wintertime, usually in fall and spring. Oxygen distribution is one of the factors that affect a lake's turnover. Oxygen is supplied to the lake's bacteria from the phytoplankton, which undergoes photosynthesis in the upper water layers due to the presence of light on the water surface since sunlight reduces

with increased water depth. In the winter, when there is little or no sunlight, bacteria consume oxygen in the sediments at the bottom of the lake, which releases nutrients from the decomposition of debris. Temperature changes and wind forces during the spring and fall are the driving forces for the water layers to mix. This phenomenon allows for the circulation of oxygen from the upper water layer known as the epilimnion and the bottom water layer called the hypolimnion. When the lake is unable to mix, an anoxic condition is created in the hypolimnion with fewer nutrients in the epilimnion impacting the productivity of phytoplankton [78].

Water bodies including lakes and rivers can also be impaired by pollutants emanating from highway stormwater runoff, industrial waste discharges, and agricultural activities, as well as municipal and residential discharges. With increasing urbanization and climate change, impairments to some water bodies continue to worsen, exposing more than half of the world's water bodies to a myriad of anthropogenic activities that ultimately destroy ecological environments and impair public health [79–81]. Most of the stormwater discharges into freshwater bodies are largely untreated and about 80% of the wastewater discharged from municipalities and industries released worldwide ends up in freshwater bodies [66]. The environmental damage caused by these pollutants is signifcant and measures need to be taken to control the rate of pollution.

Studies have looked at effective ways of reducing the amount of WQPs. One such study is the use of chitosan and the effectiveness of chitosan as a bio-coagulant in shrimp washing wastewater on three WQPs, namely, color, turbidity, and TDS. Chitosan is an eco-friendly, non-toxic, reactive natural bio-coagulant, and renewable polysaccharide obtained from the chitin deacetylation used for water and wastewater purification. Chitosan solution effectiveness was measured by computing the percentage decrease in the three WQPs. Analysis showed about a 54% reduction in TDS as opposed to an 84% reduction in color and an 83% reduction in turbidity [82]. A similar study by [83] on the effectiveness of chitosan in the removal of turbidity and bacteria from turbid waters showed a removal efficiency of >74% for turbidity at a pH of 7.0–7.5. Additionally, chitosan significantly reduced the required dosage of the primary coagulant required by more than 50%. Chitosan was also found to have reduced bacteria at 2–4 log units (i.e., 99 to 99.99%) within the first 2 h of treatments. Efficiency in the removal of *Escherichia coli* (*E. coli*) was found to be better than for *S. faecalis*. Bacteria reduction of 2–4 long units, i.e., 99–99.99%, was obtained within the first 1 to 2 h of treatment. Overall results indicate that *E. coli* was removed better than Enterococcus faecalis (*S. faecalis*).

Monitoring of water quality is carried out through conventional methods such as field measurement and laboratory analysis or RS applications. The following paragraphs summarize the water quality monitoring efforts as performed by past researchers.

Researchers in [84] investigated the use of satellite imagery for water quality studies in the New York Harbor in the US. This study compared in situ data collected from routine sampling with images from Landsat 5 Thematic Mapper (TM) and MODIS sensors and found a strong correlation between Landsat 5 TM red of bandwidth 0.63–0.69 µm reflectance and turbidity (R^2 of 85% for a sample size of 21) and chlorophyll-a concentration (R^2 of 78% for a sample size of 16). Thus, turbidity increments due to runoff and spring tide resuspension in Newark Bay were identified and mapped based on the reflectance in the red band of Landsat 5 TM images. There was no correlation between the Terra MODIS images and the in situ chlorophyll-a concentration observation. The MODIS images were not directly useful for determining the concentration of chlorophyll-a in the study area.

Researchers in [85] performed studies on water quality monitoring in support of the EU WFD in the Gulf of Finland using RS techniques. The study aimed to extract the spatial distribution of water quality with a focus on nitrate concentration in support of the EU WFD. Results show that the value of nitrate concentration was below 25 mg/L, which is an indication of significantly less affected quality when compared to most of the countries in Europe. Nitrates are important species in water bodies for several years because they are associated with Phosphorus (P), which is a cause of eutrophication in water bodies [50].

Chlorophyll-a concentration is another indicator of algal biomass leading to eutrophication that may impact the ecological functions of water ecosystems [86].

Researchers in [35] assessed water turbidity in the Alqueva reservoir located in the south of Portugal using MERIS images. The study proposed a linear empirical algorithm of the green and blue spectral bands with a correlation coefficient (R) of 0.96 to estimate surface water turbidity.

Researchers in [87] performed a study using UV–visible RS reflectance to assess the spectral slopes of the absorption coefficient of colored dissolved and detrital material (CDM). In the said study, unique features of hyperspectral RS reflectance in the UV–visible wavelength were observed in the various water bodies in a wide range of coastal and open ocean environments. It was established that ocean color in the UV domain was sensitive to the variation in the CDM spectral slope. It was also established that adding UV wavelengths to the ocean color measurements will improve the retrieval of the CDM spectral slope. Further analysis of the results supports the concept for UV wavelengths to be included in the next generation of satellite ocean color sensors.

Researchers in [88] applied unpolarized Raman spectra for the determination of salinity and temperature from a natural water sample in Australia. The results demonstrate that Raman spectra of both temperature and salinity can be measured with RMSEs below 0.2 °C for temperature and 0.6 Practical Salinity Units (PSU) for salinity. The Raman spectra showed potential in determining both temperature and salinity at the same time using a numerical model based on multiple linear regressions (MLR). Results showed that both salinity and temperature have a similar influence on the spectra signatures. An increase in both parameters causes a corresponding decrease in the signal intensity.

Researchers in [66] assessed the impact of effluents on the quality of a river body and quantified the various water quality indicators such as physical, bacteriological, and chemical parameters. Knowing the concentration of these parameters aids in assessing the quality of water. While the bacteriological indicators include total coliform and E. coli, the physical indicator includes TDS, TSS, EC, pH, Total hardness (TH), DO, Biochemical oxygen demand (BOD), and chemical oxygen demand (COD), as well as the chemical parameters of various cations and anions.

Researchers in [89] developed a numerical model to estimate the turbidity for the Tennessee River and its tributaries in southeast Tennessee using Landsat 8 OLI imageries and near real-time in situ measurements. The study establishes a nonlinear regression-based numerical model using the red band (band 4) surface reflectance values of the Landsat 8 OLI sensors with bands of 0.64–0.67 μm wavelength in the estimation of turbidity in the study area. The turbidity estimation provided high accuracy with R^2 of 97% and RMSE of 1.41 Nephelometric Turbidity Unit (NTU). Images acquired on various dates were used to test the predictive performance of the model, which generated a promising R^2 of 0.94.RS methods have also been used to successfully estimate several other parameters, including suspended solids, Secchi disk, total phosphate, nitrogen, nitrate-nitrogen, dissolved inorganic nitrogen (DIN), and phytoplankton [17,21,24,45,81,90,91].

2.3. Remote Sensing

This subsection describes remote sensing systems, the principles used, and their applications in water quality monitoring.

2.3.1. Remote Sensing Systems

RS systems have been used to acquire images with solar reflectance spectral bands which are utilized for several studies including water quality, snow mapping, and plant water content based on light scattering properties of the remote sensors. RS systems used are categorized as microwave and optical systems and further divided into active and passive sensors described in the subsequent paragraphs [92–96].

Microwave and optical RS technologies are two technologies used in various studies including water quality monitoring. Optical RS sensors collect data in the visible, near-

infrared, and shortwave infrared regions of the electromagnetic spectrum, but microwave sensors use a longer wavelength (cm to m), which makes them able to penetrate through cloud cover, dust, haze, and all kinds of rainfall except the heaviest rains. The longer wavelengths of microwave sensors make them unsusceptible to atmospheric scattering, which impacts shorter optical wavelengths and makes it possible for them to detect microwave energy under all weather and environmental conditions at any time [97–99].

The following subsection describes microwave and optical remote-sensing technologies.

Microwave Remote Sensing

Microwaves are the portion of the electromagnetic spectrum with a wavelength between 1000 μm and 1 m that fall within regions of electromagnetic radiation that are almost unimpeded by the atmosphere. Microwave RS is categorized as active, also known as a non-optical sensor, and passive remote, also called an optical sensor. Optical sensors depend on the energy of the sun, unlike non-optical sensors, which produce their energy. Although most studies have measured WQPs using optical RS, there is an opportunity to measure these parameters from the microwave region of the electromagnetic spectrum [92,97,98,100]. Passive microwave sensors detect the emitted energy within their field of view. Active microwave sensors are those sensors that provide their source of radiation to illuminate their target. They are grouped as imaging and non-imaging with a common form of imaging active microwave sensors being RADAR; non-imaging active microwave sensors include scatterometers and altimeters [98].

Active microwave sensors send pulses of electromagnetic radiation, particularly microwave radiation. The sensor then records the energy that is scattered back or reflected. Properties of the reflected energy received at the antenna of the sensor depend on its distance from the antenna, target properties, and the wavelength of the signal received. Some examples of active sensors include Radio Detection and Ranging (for example Synthetic Aperture Radar (SAR)) and Light Detection and Ranging (LIDAR). These sensors are used in managing disasters, precision, agriculture, and exploring crime [99,101–103]. The SAR is a well-developed non-optical microwave sensor that operates by recording the amount of energy reflected after interacting with the Earth. Microwave sensors have been used to effectively monitor and solve environmental issues in different applications. They have been used in the study of crops, forest cover, snow ice, soil moisture, hydrological processes such as floods and rainfall measurements, water surface pollution, the productivity of natural and agricultural ecosystems, and surface temperature detection of anomalies among others [92,93,98,100]. An example of a rainfall sensor is the Tropical Rainfall Measuring Mission (TRMM). These sensors have moderate spatial resolution compared to visible and infrared satellite sensors and present an effective means of measuring rainfall, unlike conventional methods. Conventional methods of measuring rainfall such as a network of rain gauges suffer major limitations due to inappropriate spatial coverage for the capturing of spatial variations in the rainfall [100,101]. The energy recorded by the passive microwave RS can be emitted, reflected, or transmitted from the surface. Passive microwave sensors are therefore mostly categorized by low spatial resolution [98].

Passive microwave radiometers and active SAR are commonly used for the RS of soil moisture and snow water equivalent (SWE). Studies have explored the usefulness of microwave signals for the determination of the surface soil layer. Microwave bands of wavelength ranging from 0.3 to 30 cm are noted to be effective in soil moisture measurement. The microwave sensor however has a major drawback in soil estimation, which is the poor surface penetration of its signals through forest canopies and vegetation covering the soil surface [101,104]. There are known satellite microwaves including the Soil Moisture and Ocean Salinity (SMOS) by the ESA and Soil Moisture Active Passive by the National Aeronautics and Space Administration (NASA) that have been explored in studies [104].

Optical Remote Sensing

Optical RS sensors are mainly passive sensors that make use of the sun's energy. The USGS Landsat, NASA'S MODIS, and the ESA's Sentinel-2 among many others are some optical remote sensors that have been used by several scientists including water researchers for monitoring and managing water resources [99]. This research focuses on passive RS sensors. Passive sensors can be either airborne or spaceborne sensors based on the platforms launched. Images from these sensors can be multispectral or hyperspectral based on the spectral and spatial resolutions as described in the subsequent subsection.

Spectral Imaging

Spectral imaging is the acquisition of several digital images at a different and well-defined number of optical wavelengths [105]. The passive optical remote sensors are categorized as multispectral or hyperspectral images based on the spectral resolution of the sensors used [103].

Multi and hyperspectral RS images have been used in several studies including water and land observation monitoring. Hyperspectral and multispectral satellite missions offer the opportunity for the detection of species-specific spectral features. This functionality of the sensors was postulated as far back as the 1990s and is a reality today [106]. Multispectral systems collect data in 3–10 spectral bands in a single observation from the visible and the near-infrared range of the electromagnetic spectrum. The spectral bands of multispectral bands range from 0.4 to 0.7 μm for red-green-blue, and infrared wavelengths within the range of 0.7–10 μm, or more for near, middle, and far infrared [5,8]. The use of multispectral images is, however, restrictive because the spectral resolution of the images influences the quality and quantity of the information they can provide [107].

Several multispectral sensors have been successfully used in the estimation of several WQPs. These include Landsat sensors, which have been used for the estimation of TSM, COD, and TP [5,8]. There have, however, been advances in sensor development through the development of hyperspectral sensor technologies to overcome the limitations of multispectral sensor systems over the past two decades. Hyperspectral systems can collect and store several hundred spectral bands in a single acquisition producing much more detailed spectral data and high spectral resolutions in the third dimension. They have been widely applied in medical imaging, processing, food safety testing, and agricultural yield [103,108,109]. Hyperspectral RS applications offer an effective mechanism for frequent, synoptic water quality monitoring over a large spatial extent [110]. They have been used in several studies including studies to distinguish between cyanobacterial and algal blooms in inland waters. Several hyperspectral sensors have been developed and have been applied in several studies. Some of the hyperspectral satellite missions include NASA's Plankton, Aerosol, Cloud, and ocean Ecosystem (PACE), Germany's Environmental Mapping and Analysis Program (Nmap), ESA's Fluorescence Explorer (FLEX), Italy's PRecursore IperSpettrale della Missione Applicativa (PRISMA), and India's Hyperspectral Imaging Satellite (HySIS) [106]. Other miniature hyperspectral sensors used for image acquisitions and monitoring missions include Norway's HySpex VNIR, US' Micro- and Nano-Hyperspec, and Germany's Fire- flEY, which can be installed on manned or unmanned airborne platforms such as Unmanned Aerial Vehicle (UAVs), airplanes, or helicopters [103]. There are different hyperspectral cameras for image acquisition. These include pushbroom, whiskbroom, and snapshot cameras. The principle used by each hyperspectral sensor is a function of its ability to obtain the whole picture referred to as a snapshot at one time, one point of the picture known as whiskbroom, or one line of the picture called pushbroom [103].

Hyperspectral sensors collect 200 or more bands, enabling the construction of a continuous reflectance spectrum for all the pixels in the scene. Hyperspectral RS has been applied in a variety of water resource studies including flood detection, water quality monitoring, wetland mapping, estimation of bathymetry, land-use and vegetation classification, and evapotranspiration among others [108,111]. Despite the emergence of hyperspectral images,

multispectral sensors have been the preferred sensors for the mapping and monitoring of WQPs including salinity and TSS due to the low cost of image acquisition [107].

Airborne and Spaceborne Sensors

Sensors used in RS applications are grouped into two main characterizations based on the platforms in which they are installed. These categories are space and airborne sensors. Spaceborne sensors are those carried by satellites or spacecraft to areas outside the Earth's atmosphere. Examples of spaceborne sensors include Landsat satellite, Advanced Spaceborne Thermal Emission and Reflection Radiation (ASTER), Moderate Resolution Imaging Spectroradiometer (MODIS) Sensor, GeoEye, and IKONOS among others. Airborne sensors are mounted on platforms flown within the Earth's atmosphere. These platforms include boats, helicopters, aircraft, or balloons. Both airborne and spaceborne sensors have been used in past studies to examine a wide range of WQPs since the early 1970s [112]. Airborne sensors are hyperspectral passive sensors that measure the reflectance of solar radiation throughout the visible, near-infrared, and mid-infrared, and thermal regions of the electromagnetic spectrum. Images acquired are numerous but narrower. Spaceborne are also passive sensors that cover a broader geographic area compared to the coverage by airborne sensors. Spaceborne sensors make use of the constant orbital patterns of the satellite they are launched on. Images acquired by spaceborne sensors can either be multispectral or hyperspectral. The choice of a particular sensor to be used in a study depends on spectral properties and associated strengths and limitations [8].

The strengths and limitations of airborne and spaceborne sensors used in water quality monitoring are outlined [8].

The strengths of airborne RS sensors include:

- Spectral and spatial resolutions: airborne sensors have higher spectral and spatial resolutions making them appropriate for the measurement of WQPs. Hyperspectral airborne sensors produce images that allow for more detailed spatial and spectral models for the accurate classification of an image.
- Flexibility in terms of configuration: airborne sensors have higher flexibility in terms of their configuration in terms of spectral range, number bands, and wavelength. The time of survey for any project work is not fixed. There is no repeat cycle as in the case of spaceborne sensors.
- Larger geographic areas: airborne sensors can operate at higher altitudes covering a larger geographic area, and hence are suitable for regional water quality monitoring.
- Monitoring of small water bodies: airborne sensors can assess small water bodies including rivers, estuaries, ponds, and tributaries.

Airborne sensors however present the following limitations:

- Greater planning: there is a need for greater planning ahead before the airborne survey. Considerations need to be made for external factors including air traffic, weather, flight line orientations, and solar radiation.
- Cost: airborne surveys are more cost-intensive compared with spaceborne sensors. Sensitive detectors, large data storage capacity, and fast computers are needed for the image processing of airborne sensors.
- Altitude: airborne sensors usually cover smaller areas as compared to spaceborne sensors due to the lower altitude of image acquisition.

The strengths of spaceborne RS sensors include:

- Cost: spaceborne sensors produce images at typically zero to little cost and can be used for large-scale monitoring of water quality.
- Less complexity with image processing: compared to airborne sensors, processing the spaceborne image is less complex.
- Multi-temporal studies: spaceborne sensors have a revisit frequency ranging from daily to monthly making them useful for multi-temporal scale monitoring of the trends and variations in WQPs.

- Coverage of large geographic areas: spaceborne sensors can cover large geographic areas making them suitable for moderate, regional, and global water quality monitoring.

Limitations in the use of spaceborne sensors include:

- Cloud constraints: spaceborne sensors are faced with enormous limitations when a project requires a cloud-free image.
- Overestimation of water parameters: empirical and semi-empirical approaches in analyzing multispectral images by spaceborne sensors may lead to overestimations at areas where there is a contribution of reflectance from the bottom to the water leaving reflectance.
- High-resolution images acquired are costly. The limitation with coverage: there is a limitation with coverage of the electromagnetic spectrum by spaceborne sensors. Some bands such as middle infrared and thermal bands may not be covered, which may impact the accuracy of the estimation of WQPs.

Airborne sensors provide either hyperspectral or multispectral images depending on the sensor used in the image acquisition. Some of the airborne sensors used in RS applications are summarized as follows [8,16].

1. Airborne Visible Infrared Imaging Spectrometer (AVIRIS): This sensor is manufactured by NASA Jet Propulsion Lab with a hyperspectral image with 224 bands. This image has a 17 m resolution with a spectral range of 0.40–2.50 μm. The sensor utilizes the whiskbroom scan system.
2. Hyperspectral Digital Imagery Collection Experiment (HYDICE). This sensor is manufactured by the Naval Research Lab with a pushbroom scan system. This is also a hyperspectral image with 210 bands with a spectral range of 0.40–2.50 μm and a spatial resolution of 0.8 to 4 m.
3. Airborne Prism Experiment (APEX). This sensor is manufactured by VITO and produces up to 300 hyperspectral bands with a pushbroom scan system. The spatial resolution of images produced ranges from 2 to 5 m and the spectral range of 0.38–2.50 μm.
4. Compact Airborne Spectrographic Imager (CASI-1500). This sensor is manufactured by ITRES Research Limited and produces up to 228 hyperspectral bands of spectral range 0.40–1.00 μm and a spatial resolution of 0.5–3 m with a pushbroom scan system.
5. Multispectral Infrared and Visible Imaging Spectrometer (MIVIS): This sensor is manufactured by Daedalus Enterprise Inc., USA, and produces multispectral images of visible, near-infrared, mid-infrared, and thermal bands. The sensor operates on the whiskbroom scan systems with resolutions ranging from 3 to 8 m depending on the altitude.
6. Airborne Imaging Spectrometer (AISA). This sensor is manufactured by Spectral Imaging and produces hyperspectral bands of up to 288 bands with a spatial resolution of 0.43 to 0.9 μm. Images have a spatial resolution of 1 m. The sensor operates on the pushbroom scan system.
7. Digital Airborne Imaging Spectrometer (DAIS 7915). This sensor is manufactured by GER Corporation and produces hyperspectral bands with a spatial resolution of 0.43 to 12.30 μm. Images have a spatial resolution of 3–20 m depending on the altitude. The sensor operates on the whiskbroom scan system.

A variety of spaceborne or satellite sensors are used in RS applications. Images from sensors on US-government-funded satellite platforms are generally available at no cost to the user. Each sensor has different spatial, spectral, radiometric, and temporal resolutions. The spatial resolution defines the surface area, and it is represented by the pixel or cells. The spectral resolution measures the sensor's ability to resolve features in the electromagnetic spectrum. The radiometric resolution measures the sensor's potential to record varying brightness levels, while the temporal resolution measures the amount of time, usually in days, it takes satellite sensors to revisit a particular point on the surface of the earth [113].

The following paragraphs highlight some widely used remote sensors used in water quality monitoring.

Some of the widely used sensors are summarized below.

1. Landsat satellite images: Landsat programs are joint efforts of the USGS and NASA for Earth Observation and have been in existence since 1972. Landsat images have been used by stakeholders in many applications such as land use planning, natural resources management, public safety, climate research, natural disaster management, home security, and agriculture, among others [114]. The Landsat 8 Operational Land Imager (OLI), Landsat 7 Enhanced Thematic Mapper (ETM+), and Landsat 5 TM have all been used in water quality monitoring efforts. The Landsat 9 sensor has a 14-bit quantization, which can differentiate 16,384 shades, i.e., a brightness uncertainty of $\pm$0.006%) at a given wavelength. The Landsat 8 OLI sensor captures data over a 12-bit instrument with improved precision in radiometry. The sensor captures images with the overall improvement in the signal-to-noise ratio, which translates to 4096 grey levels (i.e., a brightness uncertainty of $\pm$0.024%). Landsat 1 to 7 sensors capture data with 256 grey levels (i.e., a brightness uncertainty of $\pm$0.4%) over an 8-bit dynamic range. The Landsat 8 OLI data with 12-bit are scaled to 16-bit and made available in the form of level-1 data products. These are scaled to 55,000 grey levels from the 65,536 grey levels, which can be subsequently rescaled with radiometric coefficients, which come with the product metadata file (MTL file). The rescaling is performed to the Top of the Atmosphere (TOA) reflectance and or radiance [115,116].
    i. Landsat 9 OLI/TIRS: The Landsat 9 sensor is the latest series of Earth-observing satellites launched on 27 September 2021, and its data are publicly available (Yang et al., 2022). The sensor was launched from Vandenberg Air Force Base, California, USA, onboard a United Launched Alliance Atlas V 401 rocket and it is an improved replica of the Landsat 8 sensor. It carries the Operational Land Imager 2 (OLI-2), built by Ball Aerospace & Technologies Cooperation, Boulder, CO, USA, and the Thermal Infrared Sensor 2 (TIRS-2), built at the NASA Goddard Space Flight Center, Greenbelt, MA, USA. The Landsat 9 OLI-2 provides images consistent with Landsat 8 spectral, spatial, geometric, and radiometric qualities. It has nine spectral bands over a 185 km swath of 30 m resolutions for all bands except for the panchromatic band, which is 15 m, at a maximum ground sampling distance (GSD) both in and cross tracks. Landsat 9 offers a 16-day revisit earth coverage and an 8-day offset with Landsat 8. It acquires more than 700 scenes per day [117]. The sensor was launched to continue with the collection, distribution, and archival of multispectral imagery offering users the synoptic, global, and repetitive coverage of the Earth's surface for the detection of natural and human-induced changes on a spatiotemporal scale [117].
    ii. Landsat 8 OLI/TIRS: The Landsat 8 carries the OLI and Thermal Infrared Sensor (TIRS) sensors. It was previously called the Landsat Data Continuity Mission (LDCM) and was launched on an Atlas-V rocket from Vandenberg Air Force Base, California, USA, on 11 February 2013. Landsat 8 OLI has nine spectral bands. Studies have used some of these bands and their combinations for water quality estimations. All the bands have a spatial resolution of 30 m, except band 8 with a finer spatial resolution of 15 m. A 30 m resolution means each pixel of the image provides an average reflectance value recorded of an area of 900 m^2 (30 m by 30 m) [89]. Landsat 8 OLI is available by the United States Geological Survey (USGS) on 16 days of repeat time with an equatorial crossing time of 10:00 am $\pm$ 15 min mean local time [116,118]. The Landsat 8 OLI sensor acquires around 740 scenes in a day on the Worldwide Reference System-2 (WRS-2) path/row system. It has a swath overlap that varies from 7% at the equator to about 85% at extreme latitudes. Each scene size is 114 mi $\times$ 112 mi [116].
    iii. Landsat 7 Enhanced Thematic Mapper (ETM+): The Landsat 7 was launched from Vandenberg Air Force Base, California, USA, on 15 April 1999, with a

repeat cycle of 16 days. The Landsat 7 carries an improved version of the Thematic Mapper I instrument, which was onboard Landsat 4 and 5. ETM+ sensor Landsat 7 ETM+ data collected since 2003 have gaps caused by the Scan Line Corrector (SLC) failure. Each scene of this image is 185 km wide. Landsat 7 images are delivered in 8 bits with 256 grey levels [119]. Landsat 7 ETM+ is also available by the USGS on 16 days repeat time with an equatorial crossing time of 10:00 am ± 15 mean local time [120,121]. All the bands have a 30 m resolution, except band 6 and band 8 with 60 m and 15 m resolutions, respectively [119].

iv. Landsat 5 TM: These data sets consist of seven bands with 30 m spatial resolutions for all bands except band 6, which has 120 m resolutions and, in turn, is resampled to 30 m. This sensor was launched on March 1, 1984, from Vandenberg Air Force Base in California, USA, with its data products quantized to eight bits. It carries both the Multispectral Scanner (MSS) and the TM instruments. The sensor delivered data for close to 29 years and was retired on 5 June 2013 [121–123]. Landsat 5 TM images are delivered in 8 bits with 256 grey levels [124].

2. RapidEye images: The RapidEye sensor was launched on 29 August 2008, with a 6.5 m spatial resolution. This sensor produces images used in a variety of applications, including agriculture, engineering, construction, mining, and cartography. The RapidEye sensor has five (5) spectral bands and a spacecraft lifetime of 7 years. It has a 5.5-day revisit time off-nadir and at nadir, respectively, and an approximate equator crossing time of 11:00 am local time. It has a swath width of 77 km, a camera dynamic range of 12 bits, and an image capture capacity of 5 million km^2/day. The RapidEye constellation was retired on 31 March 2020.
3. Advanced Spaceborne Thermal Emission and Reflection Radiation (ASTER): The National Aeronautics and Space Administration (NASA) launched the ASTER sensor on the Terra satellite in December 1999. It has an equatorial crossing time at 10:30 a.m. local time with 16 days of repeat time. It has a resolution of 15, 30, and 90 m depending on the bands with quantization levels of 8 bits for the 15 and 30 m resolution bands and 12 bits for the 90 m resolution. ASTER is a collaboration between NASA, Japan's Economy Ministry, Trade and Industry, and Japan Space System. ASTER data are used in the mapping of land surface temperature, elevation, and reflectance Additionally, they are used in applied geology, soils, hydrology, ecosystems dynamics, and land cover change studies [125]. ASTER is made of different subsystems, namely, the Visible and Near-infrared (VNIR), SWIR, and Thermal Infrared (TIR). Each of these subsystems collects data in a separate set of wavebands with each set having its spatial resolution. The sensor has fourteen different bands with varying spatial resolutions for each subsystem.
4. Moderate Resolution Imaging Spectroradiometer (MODIS): The first MODIS instrument was launched aboard NASA Terra in December 1999, with the second instrument launched in May 2002 aboard the NASA Aqua platform. These data have been available since February 2000 and June 2002, respectively, for the Terra and Aqua platforms. The Terra and Aqua satellite platforms have local equatorial crossing times at 10:30 a.m. and 1:30 p.m., respectively [126,127]. The MODIS sensor has a repeat cycle of 16 days and 12-bit quantization. MODIS data consist of 36 spectral bands with varying wavelengths and spatial resolutions. The MODIS sensor has 250 m spatial resolution for bands 1 and 2, 500 m for bands 3–7, and 1 km for bands 8–36. The wavelength of bands 1 to 19 ranges from 405 to 2155 nm, with bands 20–36 ranging from 3.66 to 14.28 μm. MODIS images are utilized in studying and understanding environmental phenomena, and dynamic variations in inland, ocean, and the lower atmosphere [127]. Although the MODIS data with medium resolution (i.e., 250 and 500 m resolutions) were originally designed for land studies and cloud monitoring and have lower sensitivities than MODIS ocean bands. The moderate resolution

MODIS was compared with Landsat 7 ETM+ and Coastal Zone Color Scanner (CZCS), and SeaWiFS in a study and were found to provide sufficient sensitivity for water application data. The MODIS Ocean band (i.e., 1 km resolution) was found to be 3 to 6 times more sensitive than the SeaWiFS bands, which makes it possible for them to detect subtle ocean features. Compared to Landsat 7 ETM+ bands, the moderate resolution bands of MODIS (250 and 500 m) are found to be more sensitive with nearly twice the sensitivity of CZCS blue-green bands. MODIS moderate resolution bands are hence expected to be as useful as CZCS for coastal ocean studies [128].

5. Sentinel-2 MSI: Several group efforts led by the Airbus Defense resulted in the design and building of the Sentinel-2 sensor. The Sentinel-2 satellites are a constellation of the European Space Agency (ESA) and were launched on multispectral scanners [129]. The Sentinel-2 sensor comprises two identical satellites, namely, Sentinel-2A and Sentinel-2B, in the same sun-synchronous orbit. These satellites are separated at an angle of 180° from each other with a mean orbital altitude of 786 km. The crossing time of the sentinel sensor at the descending node is 10:30 am Mean Local Solar Time (MLST). The sensors were launched on a Vega rocket from Kourou in French Guiana on 23 June 2015, and 7 March 2017, respectively, for the Sentinel 2A and 2B [130,131]. Sentinel-2 images are used in the study of water quality, impervious surface mapping, monitoring of land ecosystems and land-use land cover (LULC), forest management, agriculture, and disaster mapping [129,131–133]. The sensor has 10 days of revisit time with one satellite and 5 days of revisit time with the two satellites, at the equator under cloud-free conditions [134]. The sensor has a swath width of 290 km. The Sentinel-2 has a 12-bit radiometric resolution and spatial resolution ranging from 10 m for bands 2, 3, 4, and 8; 20 m for bands 5, 6, 7, 8a, 11, and 12; to 60 m for bands 1, 9, and 10, with wavelengths varying from 442.7 to 2202.4 nm for band 1 to 11, respectively [113].

Some of the sensors used in the estimation of WQPs are summarized in Table 1 for optical sensors and 2 for microwave sensors. Tables 1 and 2 present their year of launch, and the spatial, temporal, and spectral resolution to aid researchers in their decision on what sensor to use in their studies [5,6,8,16,40,43,135–137]. Microwave sensors have been used in the measurement of WQPs such as sea surface temperature (SST) and sea surface salinity (SSS). These parameters are important in determining the density of seawater, which is a critical indicator driving the currents of the ocean. Ocean circulation is a critical phenomenon to analyze global water balance, evaporation rates, and productivity forecast models [16].

2.3.2. Characterization of Water Quality Parameters

WQPs are grouped as optically active and non-optically active parameters for RS studies. Optical active water parameters are those parameters that are likely to impact the optical characteristics measured by RS sensors while non-optically active parameters are those parameters that are less likely to influence the optical characteristics measured by the RS sensors [138]. Examples of optically active parameters include suspended particulate matter (SPM) or sediment concentrations, CDOM, turbidity, and chlorophyll-a concentrations. Non-optically active parameters on the other hand include TP, TN, COD, DO, and TDS [138,139]. Studies have also proposed two classifications of water bodies based on reflectance ratios at 443 and 550 nm namely Case I and II waters [47]. Case I water is water with reflectance ratios at 443 and 550 nm greater than one, while Case II waters is water with reflectance ratios of at 443 and 550 nm less than one. The optical properties of Case I waters are mainly influenced by phytoplankton and their covarying compounds including CDOM and detritus. Case II waters, on the other hand, are optically deep and complex and have their non-optically active parameters determined by constituents such as mineral particles. The concentrations of these constituents do not covary with phytoplankton [47,140].

Table 1. Optical Satellite Sensors used in WQP Estimations and their specifications.

Satellite Sensor	Year Launched	Spatial Resolution (m)	Temporal Resolution (Days)	Spectral Resolution	
				Number of Bands	Wavelength (μm)
Landsat-1,2,3 MSS	1972	80	18	4	0.50–1.10
Landsat-4,5 TM	1982	30–120	16	7	0.50–2.35
Landsat-7 ETM+	1993	15–60	16	8	0.45–0.90
Landsat-8 OLI/TIRS	2013	15–100	16	11	0.43–12.51
Landsat-9 OLI/TIRS	2021	15–100	16	11	0.43–12.51
NOAA-20 VIIRS	2011	375–750	16	22	0.412–12.01
Sentinel-2 A/B MSI	2015	10–60	5	12	0.44–2.19
RapidEye	2008	5	5.5	5	0.44–0.85
SPOT-5 HRG	2002	2.5–20	2–3	5	0.48–1.75
GOCI	2010	500	1	8	0.41–0.87
ALOS AVNIR-2	2006	2.5–10	2	5	0.42–0.89
ERS-2 ATSR-2	1995	1000	3–6	7	0.56–12.00
GeoEye IKONOS	1999	3.2–0.82	~3	5	0.45–0.93
GeoEye Geoeye-1	2010	0.41–1.65	< 3	5	0.45–0.92
GOES Imager	1975	1000–4000	-	16	0.45–13.60
Japan Earth Resources Satellite Optical Sensor	1992	18.3–24.2	3	8	0.520–2.40
MERIS	2002	300–1200	1	15	0.39–1.04
Terra ASTER	1999	15–90	16	14	0.52–11.65
Terra MODIS	1999	250–1000	1–2	36	0.41–2.16
VIIRS	2011	375–750	0.5	22	0.50–12.01
HICO	2009	100	10	128	0.35–1.08
EO-1 Hyperion	2000	30	16	242	0.35–2.57
NOAA-16 AVHRR	2000	1100–4000	9	6	0.65–1.23
NOAA Polar Orbiting Environmental Satellites AVHRR	2009, 2012	1100–4000	1	6	0.580–12.5
EO-1 ALI	2000	10–30	16	10	0.43–2.35
Digital Globe WorldView-1	2007	0.5	1.7	1	-
Digital Globe WorldView-2	2009	1.85–0.46	1.1	9	0.40–0.92
NIMBUS-7 CZCS	1978	825	6	6	0.433–12.50
ENVISAT MERIS	2002	300–1200	35	15	0.390–1.04
Ziyuan 3 Multispectral Camera	2012	5.8	4–5	4	0.450–0.89
QuickBird Multispectral and Panchromatic Sensors	2001	10–30	16	-	0.450–0.90
NOAA WorldView-3	2014	0.31–0.31	1–4.5	17	0.433–12.50
CARTOSAT	2005	2.5	5	1	0.50–0.85
Digital Globe Quick bird	2001	2.62–0.65	2.5	5	0.65–1.23
OrbView-2 SeaWiFS	1997	1130	16	8	0.41–0.87

2.3.3. Remote Sensing Principles in Water Quality Monitoring

Water color and turbidity are two main optical parameters that affect the energy levels detected by RS applications. Water color increases the absorption of light in the water thereby causing a reduction in the remotely sensed signal [141]. Changes in water color can be detected by a camera or multispectral scanner. The presumption that the appearance of water is quantitatively related to water quality may not be justified, as many variables have the potential to affect the energy levels measured by satellite instruments. The variables include the time of year, sun elevation angle, aerosol and trace gas concentrations in the atmosphere, water-vapor content of the atmosphere, specular reflection of the skylight from the water surface, the roughness of the water surface, the presence of film, foam, debris, or floating plants on the water surface, water color, water turbidity, multiple reflections and scattering of solar energy in water, submerged or emergent vegetation, depth of water, and reflectance of bottom sediments [141]. Turbidity is another optically active constituent that affects the light spectrum. The effect of turbidity results in the scattering and absorption of light, preventing them from being transmitted. Turbidity has the potential to induce changes in a reservoir's vertical thermal structure. The suitability of water color and turbidity estimates using satellites can be assessed through the evaluation of the influence of hydrological and atmospheric variables. While turbidity results from colloidal or suspended substances, the color of the water is a function of water appearance

resulting from dissolved substances [35,141]. The differences in water color and turbidity affect signals in the visible and very ultraviolet and infrared wavelengths. The energy flux reaching the sensor is decreased by an increase in water color as more of the sun's energy is absorbed in the water. On the other hand, an increase in turbidity results in an increase in the energy flux reaching the sensor. This is because more solar energy is backscattered or reflected by the particles that produce turbidity [141].

Table 2. Microwave Satellite Sensors used in WQP Estimations and their specifications.

Satellite Sensor	Year Launched/ Deployed	Spatial Resolution (km)	Temporal Resolution (Days)	Spectral Resolution	
				Number of Bands	Wavelength (m)
SMOS MIRAS	2009	3.5–50	3	1	0.212
SAC-D Aquarius	2011	100	7	1	0.212
GCOM-W1 Advanced Microwave Scanning Radiometer 2 (AMSR-2)	2012	5–10	2	7	0.003–0.043
Geophysical Satellite Radar Altimeter (GRA)	1985	5	17	1	0.022
European Remote Sensing Satellite (ERS-1/2) Radar Altimeter	1991	16–20	35		0.022
ENVISAT Radar Altimeter	2002	20	30		0.022–0.094
ERS-2 SAR	1995	$\leq$0.03	35	1	0.057
Cryosat-2 SAR/Interferometric Radar Altimeter-2 (SIRAL-2)	2010	15	369	1	0.022
Sentinel 3 A/B SAR Radar Altimeter (SRAL)	2016	(0.30 × 1.64)–(1.64 × 1.64)	27	2	0.022–0.055
Japan Earth Resources Satellite L-band SAR	1992	0.018	44	1	0.235
SAtélite Argentino de Observación COn Microondas (SAOCOM-1A) L band SAR	2018	0.01–0.1	16	1	0.235
MetOp-A/B Advanced SCATterometer (ASCAT)	2007	25	1–2	1	0.057
RADARSAT-2 SAR C-band	2007	0.003–0.1	24	1	0.055
ERS-1/2 SAR	1991	50	2–7	1	0.057
QuickSCAT Ku-band scatterometer	1999	25	1–2	1	0.022
Nimbus-5, 6 ESMR	1972	2.5	1	1	0.016
Priroda-MIR IKAR	1996	1.5–7.5	1.7	5	0.003–0.040
TRMM TMI	1997	4.4	0.5	5	0.003–0.028
Aqua AMSR-E	2002	5–10	16	6	0.003–0.043
DMSP-F16 SSMIS	2003	0.013–0.069	1	4	0.004–0.015
GPM Core GMI	2014	3	2	2	0.002–0.03
Coriolis WindSat	2003	25	8	5	0.008–0.044
(Airborne) Electronically Scanning Thinned-Array (ESTAR)	1990	100	-	-	0.212
(Airborne) Scanning Low-Frequency Microwave Radiometer (SLFMR)	1999	0.5–1	-	-	0.212
Airborne Salinity, Temperature, and Roughness Remote Scanner (STARRS)	2001	1	-	-	Up to 0.212
SEASAT SMMR	1978	22–100	-	-	0.008–0.045
(Airborne) Passive Active L- and S-band Sensor	1999	0.350–1	-	-	0.212
(Airborne) Two-Dimensional Electronically Scanning Thinned-Array Radiometer	2003	0.800	-	-	0.212

The principle of RS used in the measurement of water color or turbidity is represented by Equation (1) as given by [141];

$$I_o = I_{SR} + I_A + I_B \quad (1)$$

where I_o is the solar energy that reaches the surface of the water, I_{SR} is the solar flux that is spectrally reflected at the water surface, I_A is the flux absorbed by the water, and I_B is the flux backscattered to the water surface and thereby available for remote detection. The I_{SR} is equal at all wavelengths, while the I_A and I_B produce distinctive spectral signatures depending on the water constituents. Scattering in clear water is caused by molecules and is strongly dependent on the wavelength of the light. Most of the solar energy in natural waters is in a forward direction and subsequently absorbed by the water [141]. An estimated 2% of the light flux is backscattered in clear, infinitely deep water [141]. Fifty percent of the

signal for the blue range of the spectrum comes from a depth of fewer than 15 m, with most of the signals coming from the red light at a depth of less than close to 1.1 m [141]. The portion of the backscattered energy that returns to the water surface is the signal utilized for RS. To be detected by RS, pollutants must affect turbidity, temperature, color, or wave emissivity. Dissolved constituents that add no color to water do not affect the absorption and scattering of water as measured by a multispectral scanner or spectrophotometer [141]. Dissolved colored substances increase light absorption in water and cause a reduction in the remote signal but they do not affect the light scatter. The spectral distribution of backscattered energy is however affected by additional absorption. Suspended materials on the other hand increase the backscattering of light and hence may increase the remote signal [141]. The interaction of light with these suspended materials produces a signal reflectance that is detectable from a distance. These signals can therefore be used to estimate the presence and the quantity of TSS.TSS concentration can be determined using the spectral backscattering coeefieicnt of particles as a proxy. The backscatterings of in situ measurements have been found to show susbstantial variability based on particulate loadings. The spectral properties of the water are categorized as the Inherent Optical Properties (IOPs) and the Apparent Optical Properties (AOPs). The IOPs, which describe the spectral light absorption and backscattering, are key components in linking reflectance measurements to the concentration of water parameters such as TSS. The absorption coefficient of particles in optically complex waters such as inland, coastal, and estuarine is broken into components caused by phytoplankton and those caused by non-algal particles. While the IOPs can be quantified in the laboratory, the AOPs, which include radiance and downwelling plane irradiance, are only measured using the IOPs and depend on the IOPs and the geometric structure of the radiance distribution including the wind speed, surface water structure, and atmospheric conditions [137,142,143].

2.3.4. RS Retrieval of Water Quality Parameters

RS applications in water quality monitoring of optical active parameters involve the determination of WQPs by relating them empirically, semi-empirically, analytically, or through artificial intelligence to remotely sensed reflectance [5,18,144]. The techniques used in RS are a function of the changes in the spectral signature backscattered from water. The spectral signature is related by measuring changes in empirical or analytical models to WQPs. The optimal wavelength used in WQP measurement is a function of the constituent being measured and the sensor characteristics [145]. Researchers in [5,144] outlined the different approaches by which WQPs are extracted from remotely sensed spectral data. These include:

1. Empirical method: this approach utilizes statistical relationships derived between measured RS spectral values and measured water quality. The relationship is established using regression techniques. Estimations performed by empirical models need in situ data as many parameters are likely to change between RS missions. The empirical methods are simple and easier approaches to the retrieval of water quality.
2. Analytical method: the IOPs and AOPs are used to model the reflectance. Physical relationships are then derived between the WQP, the underwater light field, and the remotely sensed radiance. This method involves the use of bio-optical and transmission models to simulate the propagation of light in water bodies and the relationship between the WQP and reflection. Parameters such as TDS are, however, determined due to their association with other colored WQPs. Salinity is only determined in microwave bands.
3. The semi-empirical methods: this approach is the combination of the empirical and analytical methods for the retrieval of WQPs. In this method, the spectral characteristics of the parameters are known. Here, the appropriate combination of wavebands is used as correlates. The spectral radiance is recalculated to above the surface irradiance reflectance, and then through regression techniques related to the WQP.

4. Artificial Intelligence (AI) methods: this is an implicit algorithm approach that differs from the three other approaches outlined i–iii. The complications from various water surfaces, WQP combinations, and sediment deposits will mean the need to use implicit algorithms for the retrieval of WQPs. AI applications capture both linear and nonlinear relationships compared with conventional statistical approaches. Studies have applied various AI applications including the neural network (NN), which is non-linear, as compared to a linear MLR model and SVM in water quality retrieval, and produced satisfactory results. ML models such as the ANN outperforms regression models such as MLR models [48,146].

2.3.5. Detection of Optically Active Parameters

Optically active parameters such as CDOM and TSS that are important for the structure and function of the ecosystem of water bodies, absorb light in the ultraviolet and visible wavelength range and influence the optical properties enabling it to be sensed from satellite observations. CDOM plays an important role in regulating light attenuation in water bodies. CDOM concentrations are conventionally estimated using the absorption coefficient. The equation for estimating absorption coefficient is presented in Equation (2) below [73,74,147];

$$a_{CDOM,m}\ (\lambda) = 2.303 \times \mathrm{A}\ (\boldsymbol{\lambda})/\boldsymbol{l} \quad (2)$$

where the value 2.303 is the conversion between the base 10 and the natural logarithm, the subscript '*m*' represents measured value, *aCDOM,m(λ)* and *A(λ)* represents the measured absorption coefficient (m^{-1}) and absorbance wavelength **λ**, and ↕ is the path length in m [147]. This equation can be narrowed to specific wavelengths of light in the near-UV and visible spectral regions (shown in Equation (3)) as the absorption coefficient of CDOM generally decreases nearly exponentially with increasing wavelengths in those regions of the electromagnetic spectrum [147].

$$a_{CDOM}\ (\lambda) = a_{CDOM,m}\ (\lambda_0)\ \exp[-\mathrm{S}(\lambda - \lambda_0] \quad (3)$$

where *aCDOM(λ)* and *aCDOM(λ_0)* represents the absorption coefficients at the observation wavelength **λ** and reference wavelength λ_0, respectively. S represents the spectral slope measured in (nm^{-1}). The *aCDOM(λ_0)* is utilized in the characterization of CDOM concentration in a specific waterbody [147].

Optical water parameters are also used to monitor several other processes aside from water quality. The high amount of CDOM and sediment loads has the potential to reduce water clarity and block radiation needed for submerged aquatic vegetation growth. Sediments, CDOM, and nutrient inputs affect the optical characteristics of estuarine waters making a color in both in situ and remote sensed a good indicator for monitoring phenomena including run-off processes [148].

The ratio between the green and red bands of satellite images is useful in the extraction of the CDOM because the reflectance is low or almost zero in the blue part of the electromagnetic spectrum due to the high absorbance by CDOM with or without interference from SPM or phytoplankton [74].

Researchers in [149] demonstrated the capability of using CDOM algorithm retrieval to monitor DOC fluxes in the Yenisei River, which is the largest Arctic River in terms of annual runoff of 630 km^3 and basin area of 2.58 million km^2. The researchers used Landsat 8 OLI and SPOT5 images in their study. It was established that the use of shorter/longer wavelength combinations can retrieve CDOM in the arctic river. The mean concentration of DOC measurement was 8.30 mg/L while the absorption coefficient of CDOM was 4.9 m^{-1}. The concentration of TSS was however found to vary from 2.63 to 19.90 mg/L. TSS was found to be highly correlated with DOC measurement with an R^2 of 74%. The best-performing model was found to be based on the green band and green-red band interaction. The model recorded an R^2 value of 76% and an RMSE of 1.21, which is an indication of high prediction. The authors recommend an extensive sampling protocol to limit the time

gaps between the RS and in situ measurements. They also propose Sentinel-2-3/Landsat 8 synergies for the reproducibility of CDOM algorithm retrievals.

Studies have also found a good correlation between the SPM concentrations and water reflectance in the green and red regions of the electromagnetic spectrum for low to moderate turbid waters [150].

A study by [73] found that the 8-bit radiometric data of Landsat 7 were not adequate for the estimation of CDOM in lakes located in southern Finland when the absorption coefficient of CDOM at wavelength 420 nm was higher than 3 m^{-1}. However, the study found the Advanced Land Imager (ALI), which is a prototype of the next-generation Landsat, to be suitable for mapping CDOM in a wider range of concentrations. Chlorophyll-a concentrations serve as differential absorbers causing a decrement in the spectral response at the blue region (450–520 nm) of the electromagnetic spectrum with reflectance being greatest at the green and red wavelengths. Suspended solids are, however, found to be associated with an increase in reflected energy at longer wavelengths (630–690 nm) [7,121].

A study was performed by [4] to estimate optical water parameters using a guided approach. The optical WQPs considered included chlorophyll-a concentration, TSM, the absorption coefficient of CDOM, SDD from Ocean and Land Color Instrument (OLCI), and MSI data at Estonian and Finnish lakes and the Baltic Sea coastal area. The study used empirical algorithms. High correlations (R) $\geq$ 0.87, were established for in situ measured optical WQPs and the parameters predicted by the optical water-type guided approach. The presence of multiple constituents such as phytoplankton, CDOM, and non-algal particles (NAP) at different compositions in inland waters has however made the use of RS applications for the monitoring of inland water quality to be less successful as compared to open oceans [47]. RS techniques can monitor optically active parameters but have limited capacity to detect and monitor optically inactive parameters such as TN and TP [48].

2.3.6. Detection of Optically Inactive Parameters

Researchers in [48] utilized optically active parameters such as chlorophyll-a, Secchi disk depth (SDD), and TSS to determine optically inactive parameters such as TP and TN concentrations in the Geshlagh reservoir located in the west of Iran using Landsat 8 OLI images.The study established that band ratios (B3/B2) and bands 3 and 4 were the most effective for the determination of chlorophyll-a concentration and were subsequently used for the prediction of TP and TN concentrations in the reservoir. Previous research established a relationship between band combinations for TN and TP predictions based on their correlations with SDD, TSS, and chlorophyll-a concentrations [48].

Retrieving optically inactive parameters using satellite visible, NIR, or IR bands such as TN, TP, pH, and COD among others is possible because of their correlation with the optically active parameters [89,138]. Researchers in [138] found that bands 3, 4, and 5 of Sentinel-2 images to be the most influential bands for the detection of TN, TP, and COD. Estimation of optically non-active parameters including TDS assumes that there is a process that (usually) co-occurs with changes in the TDS or salinity that affects a WQP that is optically active. These processes may, however, not always co-occur in the same magnitude.

2.3.7. Remote Sensing Applications in Water Quality Monitoring

Water quality monitoring involves the systematic collection and analysis of water samples to provide knowledge and information about the water body to inform critical decisions [37]. Although RS has been used since the 1980s for the synoptic and multi-temporal studying of inland water quality [34,151], it was not until the early 21st century that CHRIS Compact High-Resolution Imaging Spectrometer (CHRIS), which is an experimental multi-angle sensor with a good spatial and spectral resolution, and MERIS, which has good spectral and temporal resolutions, started to acquire good resolutions. These images allow for the development of a reliable imagery acquisition system to be

used as a water management tool [34]. The monitoring of small urban water bodies by RS applications can be challenging due to the coarse spatial resolutions of some sensors [138].

Most studies have applied sensors with shorter wavelengths in the study of many types of earth and water features including water monitoring. Some of the shorter wavelength bands include those in the visible and near-infrared. Visible radiation is that portion of the electromagnetic spectrum with a wavelength of between 0.4 to 0.7 μm, which the human eye can perceive. The near-infrared has a wavelength ranging from 0.7 to 1.0 μm [100]. This study focuses on sensors with shorter wavelengths such as visible and infrared wavelengths that have been used in the monitoring of water quality due to their high frequency of data acquisition with large-scale coverage [5].

RS techniques have been utilized in the monitoring and management of water quality. Several WQPs have been monitored with these techniques. Some of these parameters include TDS or salinity, SS, chlorophyll-a concentration, turbidity, surface water temperature, cations, and anions [8,17,42,86,152–161].

Surface WQPs are detected through different satellite reflectance values on the principle that every object has its reflectance value based on its physical properties. The use of satellite reflectance allows for a vast scope and several temporal monitoring of surface water parameters [162]. Satellite reflectance is the signal of the image on the water surface, which is a function of absorption and backscatter in the water body absorption/backscatter in atmosphere.

Studies have estimated WQPs using digital evaluations of optical satellite data at visible and near-infrared wavelengths [45]. Solar radiation can penetrate and interact with different components as it travels within the column of water in the visible and near-infrared wavelength ranges of the electromagnetic spectrum [163].

Researchers in [164] modeled the spatiotemporal changes of Lake Urmia, which, in September 2010, was the twentieth-largest lake and second-largest hypersaline lake in the world. The study was performed for the period 2000–2013 using RS images from Landsat 5 TM, 7 ETM+, and 8 OLI sensors. Their study considered various indices including the Normalized Difference Moisture Index (NDMI), Normalized Difference Water Index (NDWI), Modified NDWI (MNDWI), Automated Water Extraction Index (AWEI), Water Ratio Index (WRI), and Normalized Difference Vegetation Index (NDVI). The study found NDWI to be a better index and adopted it for spatiotemporal changes in the lake. A principal components analysis (PCA) of the multi-temporal NDWI was evaluated for the detection of surface water quality. Results show a decreasing trend in the lake surface area in the period under study. The PCA technique is useful for producing uncorrelated output bands, separating noise components, and further reducing the dimensionality of data.

Although most studies have measured WQPs using the visible and near-infrared wavelengths of the electromagnetic spectrum, there is an opportunity to measure this parameter from the microwave region of the electromagnetic spectrum. Unlike visible and near-infrared sensors, microwave sensors are less susceptible to atmospheric attenuations, making them suitable for the detection of biophysical properties including those of crops and soils, coastal areas, and extreme weather monitoring in any condition during the day or night [165,166]. Microwave sensors flown on aircraft can be used in estimating temperature distributions to about 1 °C. Similarly, salinity distribution can also be determined by microwave radiometers [167]. Microwave RS has also been explored for the estimation of several WQPs including suspended sediment concentration (SSC), SDD or Secchi disk transparency (SDT), turbidity, chlorophyll-a concentration, salinity, or TDS.

Researchers in [146] applied an empirical neural network in the estimation of WQPs such as SSC, SDD, turbidity, and chlorophyll-a concentration in the Gulf of Finland using combined optical (Landsat 5 TM) and microwave data (European RS (ERS)-2 SAR). Results indicate that the neural network was adequate in describing the nonlinear transfer function between the optical and microwave sensors and the water surface parameters. The optical and microwave sensors including the thermal band produced an R^2 of >91% for all the measured surface WQPs without the thermal bands, and the performance reduced slightly

to an R^2 of >85% of the WQPs. Thermal bands measure the emitted thermal radiance of the water body. They do not measure the sunlight reflected.

Several studies have utilized different RS sensors and techniques for the retrieval of WQPs and have achieved varying degrees of accuracy. Some of the studies that have retrieved WQPs with RS data have been summarized in Tables 3 and 4 for optically active and optically non-active parameters.

Table 3. Model Retrieval of Optically Active WQPs widely measured using RS Applications.

WQPs	Sensor/Data	Model/Algorithms	R^2	Study Area (Region/Country)	Reference
TSS/TSM/SSC/SS/SPM	MODIS	Empirical	0.89	Lake Pontchartrain, Mississippi River. Mississippi Sound (US)	[168]
TSS/TSM/SSC/SS/SPM	RapidEye, SPOT 6, Pleiades-1A	Empirical	0.65	Didipio catchment (Philippines)	[25]
TSS/TSM/SSC/SS/SPM	Landsat-4, 5 TM, Landsat 8 OLI	Semi-empirical	-	Pear River Estuary (China)	[169]
TSS/TSM/SSC/SS/SPM	MODIS	Neural Network	0.72	Bohai Sea, Yellow Sea, East China Sea (China)	[170]
TSS/TSM/SSC/SS/SPM	ALOS/AVNIR-2	Empirical	>0.70	Monobe River (Japan), Altamaha River (US), St. Marys River (US)	[171]
TSS/TSM/SSC/SS/SPM	Landsat 5 TM	Neural Network	> 0.90	Beaver Reservoir (US)	[172]
TSS/TSM/SSC/SS/SPM	MODIS	Empirical	0.83	Green Bay of Lake Michigan (US)	[173]
TSS/TSM/SSC/SS/SPM	Landsat 8 OLI	Empirical	-	Keenjhar Lake (Pakistan)	[174]
TSS/TSM/SSC/SS/SPM	Landsat 8 OLI	Empirical	>0.50	Nakdong River (South Korea)	[175]
TSS/TSM/SSC/SS/SPM	Indian Remote-Sensing Satellite (IRS-P6)	Empirical	0.94	Shitoukoumen Reservoir (China)	[176]
TSS/TSM/SSC/SS/SPM	CASI	Empirical	0.96	Tamar estuary (UK)	[177]
TSS/TSM/SSC/SS/SPM	MODIS	Empirical	0.90	Tampa Bay (USA)	[128]
TSS/TSM/SSC/SS/SPM	Sentinel-2A MSI	Semi-empirical and ML	0.80	Water Reservoirs (Czech Republic)	[178]
TSS/TSM/SSC/SS/SPM	Landsat 8 OLI	AI	>0.93	Saint John River (Canada and US)	[179]
TSS/TSM/SSC/SS/SPM	MERIS	-	-	Lake Maggiore (Italy)	[180]
TSS/TSM/SSC/SS/SPM	IRS LISS III	Empirical	>0.23	Gomti River (India)	[181]
TSS/TSM/SSC/SS/SPM	Hyperspectral Imager for the Coastal Ocean (HICOTM)	Semi-empirical	0.85	Northern Adriatic Sea	[182]
Chlorophyll-a	Landsat 5 TM	Neural Network	>0.50	Beaver Reservoir (US)	[172]
Chlorophyll-a	ALOS/AVNIR-2	Empirical	>0.70	Monobe River (Japan) Altamaha River (US), St. Marys River (US)	[171]
Chlorophyll-a	EO-1 Hyperion	Empirical	0.59	Lake Garda (Italy)	[183]
Chlorophyll-a	Landsat-5 TM, SPOT-Pan, IRS-1C/D LISS, Pan, Landsat-5 TM	Empirical	0.26	Küçükçekmece Lake (Turkey)	[184]
Chlorophyll-a	Landsat 8 OLI	Empirical	>0.50	Nakdong River (South Korea)	[175]
Chlorophyll-a	Landsat 8 OLI	Empirical	>0.34	Nakdong River (South Korea)	[175]
Chlorophyll-a	Landsat 7 ETM+	Empirical	>0.70	Rotorua Lakes (New Zealand)	[7]
Chlorophyll-a	MERIS, MODIS	Semi-empirical	>0.90	Lake Okoboji, Lakes, and Reservoirs in Nebraska, Lake Minnetonka, Choptank River (US)	[23]
Chlorophyll-a	MERIS, MODIS	Semi-empirical	0.89	Fremont State Lakes (US)	[185]
Chlorophyll-a	MERIS	Empirical	>0.90	Taganrog Bay, Azov Sea (Russia)	[186]
Chlorophyll-a	Landsat 5 TM		>0.60	Minnesota Lakes (US)	[187]
Chlorophyll-a	Landsat 5 TM		>0.80	Minnesota Lakes (US)	[187]
Chlorophyll-a	Landsat 5 TM	Neural network	>0.95	Kissimmee River basin (US)	[188]
Chlorophyll-a	Landsat 7 ETM+	Empirical and semi-analytical	0.68	Rotorua Lakes (New Zealand)	[152]
Chlorophyll-a	Sentinel-2A MSI	semi-empirical and ML	0.85	Water Reservoirs (Czech Republic)	[178]
Chlorophyll-a	PROBA-CHRIS	Empirical	0.89	Mazurian Lakes (Poland)	[189]
Chlorophyll-a	MERIS	-	-	Lake Maggiore (Italy)	[180]
Chlorophyll-a	HICOTM	Semi-empirical	0.71	Northern Adriatic Sea	[182]
Chlorophyll-a	MODIS	Empirical, Neural network,	>0.61	Chaohu Lake (China)	[190]
Chlorophyll-a	Airborne real-time cueing hyperspectral enhanced reconnaissance (ARCHER)	Analytical	-	Shenandoah River Basin (US)	[95]
CDOM	Airborne real-time cueing hyperspectral enhanced reconnaissance (ARCHER)	Analytical	-	Shenandoah River Basin (US)	[95]
CDOM	ALOS/AVNIR-2	Empirical	>0.70	Monobe River (Japan), Altamaha River (US), St. Marys River (US)	[171]
CDOM	Landsat 5 TM		>0.60	Minnesota Lakes (US)	[187]
CDOM	MERIS	-	-	Lake Maggiore (Italy)	[180]
CDOM	Ship—mounted spectroradiometer Hyperspectral data	Empirical, Analytical, Semi-Analytical	>0.65	Mississippi River and Atchafalaya River (US), The northern Gulf of Mexico	[191]
CDOM	Landsat 8 OLI	Empirical	>0.7	Saginaw and Kawkawlin Rivers (US)	[169]
CDOM	Landsat 8 OLI, RapidEye	Semi-Analytical	0.52	Lake Garda (Italy)	[151]
Turbidity	ARCHER	Analytical	-	Shenandoah River Basin (US)	[95]
Turbidity	Landsat-5 TM + SPOT-Pan, IRS-1C/D LISS + Pan, and Landsat-5 TM	Empirical	0.68	Küçükçekmece Lake (Turkey)	[184]
Turbidity	Landsat 7 ETM+	Empirical	>0.76	Rotorua Lakes (New Zealand)	[121]
Turbidity	Landsat 5 TM	Neural network	>0.95	Kissimmee River basin (US)	[188]
Turbidity	Landsat 8 OLI	AI	>0.99	Saint John River (Canada, and US)	[179]
Turbidity	Indian Remote Sensing (IRS) P6 LISS IV	Empirical	>0.11	Malad Creek (India)	[192]
Turbidity	MODIS	Empirical	0.87	Green Bay of Lake Michigan (US)	[173]
SDD/SDT	Landsat 7 ETM+	Empirical	>0.80	Rotorua Lakes (New Zealand)	[7]
SDD/SDT	Landsat 5 TM	Empirical	>0.7	Ebro river basin (Western Europe)	[193]

Table 3. *Cont.*

WQPs	Sensor/Data	Model/Algorithms	R^2	Study Area (Region/Country)	Reference
SDD/SDT	PROBA-CHRIS	Empirical	0.95	Mazurian Lakes (Poland)	[189]
SDD/SDT	MODIS	Empirical, Neural Network,	>0.45	Chaohu Lake (China)	[190]
Algal bloom	Landsat 1, 3 MSS, IRS LISS-III, IRS LISS-IV	Empirical	0.88	Sambhar Lake (India)	[194]
Algae bloom	Landsat 5 TM	Empirical, Theoretical algorithms	0.86	Guanting Reservoir (China)	[24]
EC	Worldview-2	Empirical	0.68	Lake Al-Saad (Saudi Arabia)	[195]

Table 4. Model Retrieval of Optically Inactive WQPs widely measured using Remote Sensing Applications.

WQPs	Sensor/Data	Model/Algorithms	R^2	Study Area (Region/Country)	Reference
TP	Landsat-5 TM, SPOT-Pan, IRS-1C/D LISS, Pan, and Landsat-5 TM	Empirical	0.62	Küçükçekmece Lake (Turkey)	[184]
TP	Airborne imaging data (AISA)	Empirical	>0.60	Eagle Creek Reservoir, Geist Reservoir, Morse Reservoir (US)	[176]
TP	Landsat 8 OLI	Empirical	0.80	Xin'anjiang Reservoir (China)	[196]
TP	Landsat 5 TM	Neural network	>0.95	Kissimmee River basin (US)	[188]
TP	Landsat 5 TM	Empirical	0.77	Qiantang River (China)	[197]
TP	MODIS	Empirical, Neural network	>0.24	Chaohu Lake (China)	[190]
TP	Landsat 5 TM	Empirical and theoretical	0.38	Guanting Reservoir (China)	[24]
DP	Landsat 5 TM	Empirical and theoretical	0.91	Guanting Reservoir (China)	[24]
TN	Landsat-5 TM, SPOT-Pan, IRS-1C/D LISS, Pan, Landsat-5 TM	Empirical	0.70	Küçükçekmece Lake (Turkey)	[184]
TN	Landsat 8 OLI	Empirical	>0.20	Nakdong River (South Korea)	[175]
TN	Landsat 8 OLI	Empirical	0.84	Xin'anjiang Reservoir (China)	[196]
NH_3-N	Landsat 5 TM	Empirical and theoretical	0.65	Guanting Reservoir (China)	[24]
NO_3-N	Landsat 5 TM	Empirical and theoretical	0.85	Guanting Reservoir (China)	[24]
TN	MODIS	Empirical, Neural network	>0.50	Chaohu Lake (China)	[190]
TN	Landsat 5 TM	Empirical and theoretical	0.56	Guanting Reservoir (China)	[24]
TDS/DS	Sentinel-2 MSI	Empirical	-	Guartinaja, Momil wetlands (Columbia)	[139]
TDS/DS	Landsat 8 OLI	Empirical	>55	Shatt al-Arab River (Iraq)	[28]
TDS/DS	Landsat 8 OLI	Empirical	0.64	Tigris River (India)	[198]
TDS/DS	Landsat 5 TM	Empirical	>0.83	Tigris and Euphrates Rivers (Iraq)	[145]
TDS/DS	Landsat 8 OLI	Empirical	>0.95	Tubay River (Philippines)	[199]
TDS/DS	IRS LISS III	Empirical	>0.46	Gomti River (India)	[181]
COD	Landsat 8 OLI	Artificial Intelligence	>0.93	Saint John River (Canada and US)	[179]
COD	Landsat 5 TM	Empirical	>0.63	Shenzhen Reservoir (China)	[200]
COD	IRS LISS III	Empirical	>0.28	Gomti River (India)	[181]
COD	Landsat 5 TM, Landsat 7 ETM+	Empirical	>0.66	Dongting Lake (China)	[201]
BOD	Landsat 8 OLI	Artificial Intelligence	>0.92	Saint John River (Canada and US)	[179]
BOD	Landsat 5 TM	Empirical	>0.70	Shenzhen Reservoir (China)	[200]
BOD	IRS LISS III	Empirical	>0.48	Gomti River (India)	[181]
DO	Landsat 8 OLI	Artificial Intelligence	>0.93	Saint John River (Canada and US)	[179]
DO	IRS LISS III	Empirical	>0.56	Gomti River (India)	[181]
DO	Worldview-2	Empirical	0.67	Lake Al-Saad (Saudi Arabia)	[195]
TOC	Landsat 5 TM	Empirical	>0.82	Shenzhen Reservoir (China)	[200]
pH	IRS LISS III	Empirical	>0.70	Gomti River (India)	[181]

Based on information obtained from the literature reviews, a generalized systematic overview to be utilized for any study involving the monitoring and management of water quality using RS applications is presented in Figure 1 and described in the following paragraphs.

The first approach to be employed in water quality assessment with RS involves conducting a literature review: this involves searching through literature databases on the background and the state-of-the-art work performed in the area and identifying gaps to be addressed. Some of the known databases include Web of Science™, Compendex™, Scopus™, and Google Scholar™ with keywords such as water quality, RS, and satellite sensors.

The second approach entails methodology development. This includes establishing WQPs to be measured and the identification of RS and ground truth data to be used. RS sensors include airborne and spaceborne. The sensor and image acquisition to be used depend on a lot of factors including the availability of resources and the desired need. Ground truth data sets include field measurements or laboratory analysis of the WQPs. The USGS collects several WQPs that are available for free on their website for download for any RS analysis. After obtaining RS data through drones and satellites, level 1 images need to be corrected by application of atmospheric corrections. Some of the known atmospheric

algorithms used in literature include Dark Object Subtraction (DOS) and Atmospheric Correction based on Turbidity Classification (ACbTC). These algorithms have the potential to overcome the adjacency effects caused by dark waters and bright land in the NIR bands. Atmospheric corrections are essential prerequisites needed to be performed to obtain accurate inland water information. Studies have also found that combining different RS data using merging algorithms proved to be a plausible approach for the precise retrieval of WQPs [5,202,203]. After establishing a method to be used, the next step involves model development: models are developed typically by using band reflectance in the RS image and the ground truth data.

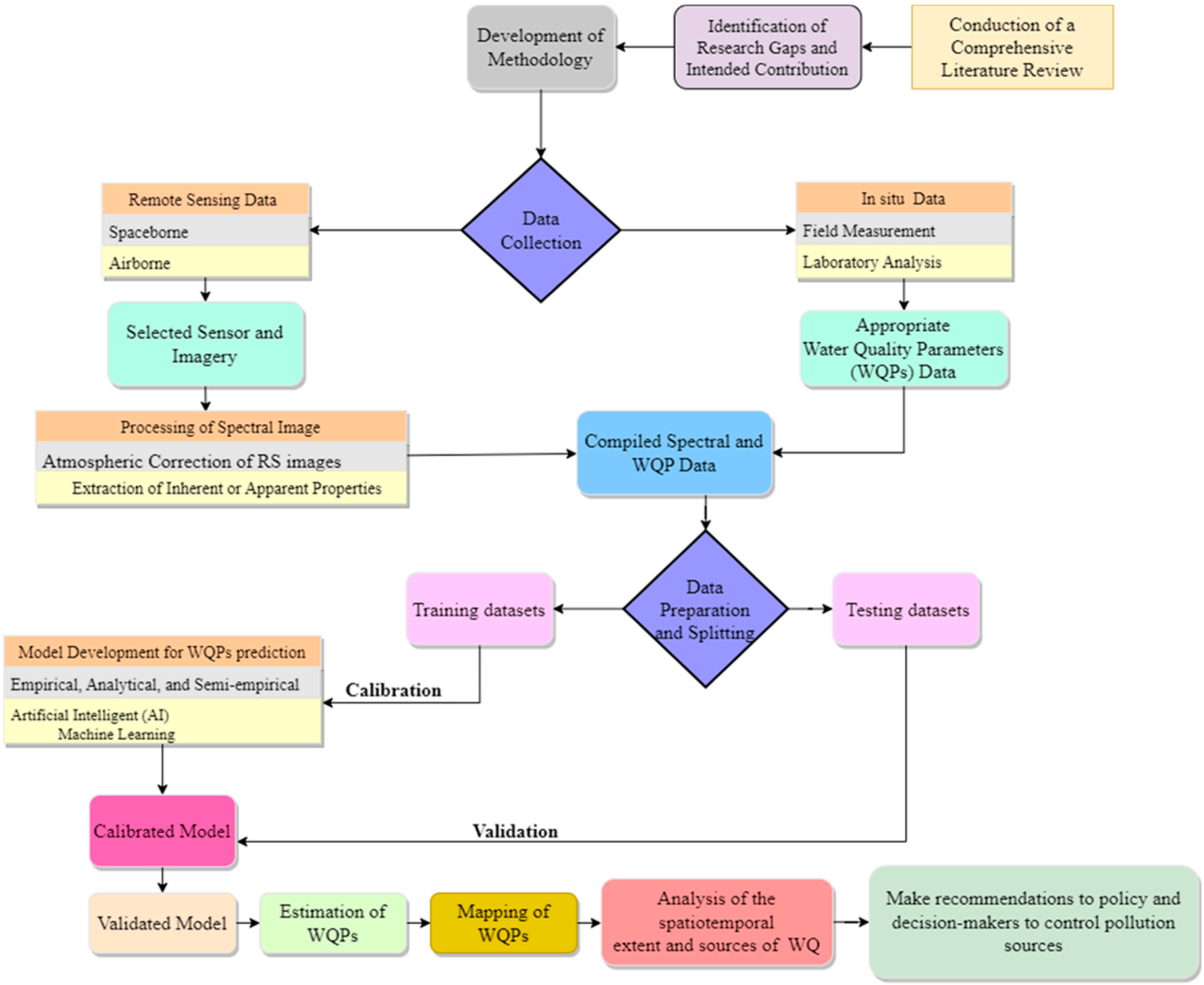

Figure 1. A proposed schematic framework to be utilized for monitoring and assessment of Water Quality using Remote Sensing Applications.

Several statistical models may be explored depending on the need of the researcher. Some of the models include empirical regression models, and machine learning techniques such as ANN, SVM, and PCA, among others. After the model is developed, models then need to be calibrated and validated. Developed models are trained and calibrated to ensure accuracy in the prediction of WQPs and evaluated using statistical metrics such as Nash–Sutcliffe Efficiency (NSE), Percent Bias (PBIAS), Root Mean Square Error (RMSE), Mean Absolute Error (MAE), and Percent Mean Absolute Relative Error (PMARE) [204–208]. The evaluated models are then used to predict and map of WQPs: WQPs are predicted using the developed models and then mapped to assess the spatiotemporal extent of water

degradation or pollution. Once the WQPs are mapped, the sources of pollution can then be analyzed; once the sources are known, proposals and recommendations can then be offered on the strategies to control the sources and the mitigating effects.

3. Strengths and Shortcomings of RS Applications

3.1. Strengths

RS techniques present the opportunity to manage and protect water resources. RS applications offer researchers and policymakers the opportunity to carry out synoptic, consistent, repetitive, detailed, and cost-effective assessments of water quality on a spatiotemporal scale compared with point-based in situ measurements [16,18]. Measurement of WQPs with RS satellite sensors can be performed at a great distance, i.e., several hundred to thousands of miles, which helps in the coverage of large areas on the ground and can observe water surfaces repeatedly [43].

The use of satellite images saves users a huge sum of money that would have been spent on field or laboratory work. The use of satellite images and improved statistical and mechanistic modeling of WQPs has been performed at local, watershed, and regional scales with a high degree of accuracy. These models also can effectively enhance the real-time detection of hydrological variability, which is key in providing early warning and rapid response to harmful algal bloom events [18].

Most satellite images are freely available, open-source data that can be accessed at no cost to the users. Different sensors offer different advantages compared to others in terms of their spatial and temporal resolutions. Comparing Landsat sensor data to sensors of higher resolution such as those aboard the SPOT, ASTER, or IKONOS satellite program still places the Landsat programs at an advantage owing to their more extensive temporal record dating back as far as the 1970s. Landsat satellites have been extensively used for water quality assessment due to their relatively low cost, and spatial and temporal resolutions. The utilization of Landsat image data has saved users a sum of about USD 3.45 billion as of 2017, with users in the United States accounting for about 59.7% [114]. The Landsat program serves as a central reference comparison focus for many different moderate and high-resolution optical satellite sensors operated by commercial and government institutions due to their associated benefits including the length of a record, availability of data, calibration standards, and global coverage. Landsat programs have influenced the development of other earth RS satellites by government agencies such as the ESA's Copernicus Program Sentinel-2 satellite constellation and private agencies' systems [114].

3.2. Limitations

Although RS satellite images offer a great tool for the monitoring of WQPs, they possess some underlying limitations that when properly addressed will improve their performance and provide many comparable results with conventional methods. The limitations of RS techniques are outlined in the following paragraphs.

Image acquisition errors may occur. The atmospheric path existing between the sensor and the water surface impacts remotely sensed reflectance, which, in turn, affects the data acquired. The interactions of the sensor's incident energy with atmospheric conditions are significant enough to impact the incoming radiance, which has the potential to compromise the image. Cloud cover, fog, and haze will blur or obscure target water bodies. Hence, they impact images collected in the visible and near-infrared regions of the electromagnetic spectrum [5,6]. As a result, atmospheric corrections need to be carried out before analysis is performed. Atmospheric corrections are important for water surfaces where the reflected light fraction is very low (i.e., not more than 10% of the radiance measured by the sensor) [18].

Atmospheric interference: This has the potential to restrict the optical signals sensed from the surface of the water bodies. The maximum penetration of light in seawater is at a depth of around 55 m near the 475 nm wavelength. At this depth, a greater percentage of incident energy on the water surface is transmitted. With increased concentrations of

sediments to about 400 ppm, light penetration reduces to about 60 cm, making only a progressively thinner layer of surface water detectable [16]. The interactions of incident energy and the atmospheric conditions are significant enough to quantitatively affect the incoming radiance and hence can comprise the results [18].

Image processing errors such as processes involved in the atmospheric corrections and pan-sharpening of satellite images may induce errors when using these images for the estimation of water quality. Satellite images with coarse spatial resolutions may possess issues related to the contamination of pixels with the land surface presenting an inaccurate spectral signature. Additionally, remote sensing image processing errors may result in an invalid detection of WQPs, bringing the accuracy of extracted WQPs into question [40]. For example, the densest areas of cyanobacteria blooms in the Baltic Sea are said to be usually masked out in chlorophyll product maps as processing errors or an atmospheric correction. This is because high reflectance in the near-infrared range of the electromagnetic spectrum is not anticipated by ocean color algorithms [209].

Studies have considered ways of improving the accuracy of their results obtained from high-resolution images through techniques such as pan-sharpening. Other studies resampled their pixel resolution such as the case of [139] where the 20 m resolution Sentinel 2 image was resampled to 10 m resolution. Pan-sharpening or downscaling, unlike conventional resampling, is a fusion technique that allows for the artificial enhancement of the spatial resolution of the image by fusing it with a higher-resolution image. Pan-sharpening introduces less spectral and spatial distortion and provides visually more coherent data compared with resampling of the pixel [210,211]. Conventional resampling of images selects the closest image pixel and preserves the input data, which has the potential to cause blockings in the pixel and location shifts [210]. The authors in the study [210] compared the results of a conventional resampling of a 30 m resolution Landsat 8 OLI to 20 m and Panchromatic-Assisted Downscaling (LPAD) or pan-sharpening of 30 m reflective wavelength bands to Sentinel-2 20 m resolution and found that the LPAD resulted in clearer object boundaries and finer spatial detail than the conventionally resampled data. Although these techniques have been applied to images, it is noted that the pan-sharpened approach alters the radiometric and spectral features of the satellite image and is only useful for image visualization and interpretation, and not for analytical purposes [211]. Researchers in [212] also noted that the sharpening procedure introduces artifacts, particularly around bright non-water pixels, and is therefore not recommended to resample high-resolution bands for noise reduction. The authors pointed out the spatial resolution of the image is its strength, and the native resolution band will produce adequate performance.

Another drawback in the use of RS techniques in the monitoring of water quality is the lack of in situ data in some areas, particularly in sub-Sahara Africa, for the calibration and validation of remotely sensed models due to associated on-site cost and high level technical expertise involved in conducting in situ water quality monitoring efforts [18]. Models developed using RS data need to be properly calibrated and validated using in situ data. The absence of in situ measurements for calibration and validation raises accuracy concerns [16,40].

Weak or inactive optical characteristics of some WQPs: Most of the WQPs detected directly by RS applications are optically active such as TSS, CDOM, and chlorophyll-a concentration. These parameters absorb light in the EM spectrum and influence water optical properties enabling these parameters to be sensed from satellite observations, unlike the optically inactive or weak optical parameters such as TDS, pH, TN, and NH_3-N, which have a low signal-to-noise ratio. The estimation of optically inactive parameters such as TDS is due to their statistical associations with other colored WQPs with which they may co-vary. Additionally, retrieval of most WQPs is performed through methods that require accurate parameterization, which may vary with the optical property of the water body [16,135].

Limitations of the sensor's spatial, spectral, and temporal properties: Other limitations that arise with the use of RS have to do with spatial, temporal, and spectral resolutions

of RS sensors. RS sensors have different spatial, spectral, and temporal resolutions, and depending on the need, it may be difficult to rely on a particular sensor to detect temporal trends, especially when they have a longer repeat cycle. An example is comparing the temporal resolutions of Sentinel-2 A/B MSI, which has a 5-day revisit time, to Landsat 8 OLI, which has a 16-day revisit time.

Airborne sensors compared with spaceborne sensors have finer spatial and temporal resolutions, but the data may, however, come at a higher cost to the user and may defeat the purpose of cost savings with the use of RS. Data from most sensors such as MODIS (250 m–1.1 km), MERIS (300 m), and SeaWiFS (1.1 km) are suitable for the effective retrieval of ocean WQPs but may not work efficiently for inland water bodies such as narrow river channels and lakes due to their coarse spatial resolutions and their low signal-to-noise ratios. Data from some sensors with high spatial resolution may not provide an effective time series of effective assessments of WQPs due to their low temporal resolutions. Those sensors with high temporal resolutions may also not support comprehensive and effective investigations owing to their coarse spatial resolutions [5].

4. Summary and Recommendations

In summary, traditional in situ methods of monitoring WQPs are not only cost-intensive but require constant laboratory and field efforts. The use of RS techniques and geospatial tools, however, provides a cost-effective approach for the assessment of WQPs on a wide spatial scale in a reliable manner in space and time. Both spaceborne and airborne RS sensors have the potential to reliably estimate WQPs. Retrieval of WQPs from RS images is performed through empirical, analytical, semi-empirical, and AI methods, as described in Section 2.3.5.

Multispectral sensors in water quality monitoring have been used widely due to the availability of their images across the globe. Their usage is said to be gaining ground in developing countries. The use of multispectral images such as MERIS in the study of small inland lakes may pose some accuracy issues due to their coarse resolution. Coarse-resolution images have only one pixel representing a large area, which is a potential source of error since each small area may have its distinct features. An example is a study to compare the Chinese high-resolution GF-1 Wide Field Imager (WFI) data with MODIS for the estimation of SPM. High consistency in the spatial distribution and concentration of SPM maps was seen between the GF-1 and Landsat 8 OLI data. More than 75% of the spatial variations were resolved by the GF-1 while only 40% were resolved by the MODIS band with 250 m resolution, indicating the limitations of using a coarse resolution image such as the MODIS [213].

The use of UAV airborne sensors is on the ascendency due to the rapid development of these sensors. Airborne-based spectrometers provide efficient and flexible solutions to underlying temporal, spectral, and spatial resolution issues associated with some satellite sensors.

Retrieval of WQPs using RS is based on the optical properties of the WQPs. Parameters such as TSS, CDOM, chlorophyll-a concentration, and turbidity can be directly determined using RS images since they are optically active. Retrieving optically weak or inactive parameters such as TDS, TN, TP, COD, and pH is possible because they have been found to correlate with optically active parameters.

Based on the literature review, the following recommendations are made for future considerations for the effective assessment of water quality.

Establishment of atmospheric correction model: When using level 1 raw satellite images, it is recommended that high-precision atmospheric correction algorithms such as DOS and ACbTC be employed to improve the accuracy of the retrieval models for water quality. UAV platforms should be used for capturing RS images without inferences from the atmosphere. When available, level 2 atmospherically corrected surface reflectance data sets should be used to minimize the potential errors associated with atmospheric corrections.

The Use of High-Resolution Images: Analyses of water quality should be performed using high-resolution satellite data. High-resolution images with shorter revisit intervals should be used for water quality assessment. Examples of high-resolution images include GeoEye IKONOS with a spatial resolution of 0.82–5 m and revisit time of 2–3 days; and Digital Globe WorldView-1 with a resolution of 0.5 m and a revisit interval of 1.7 days. Additionally, hyperspectral images should be utilized and explored for the estimation of WQPs, Examples include Airborne Visible Infrared Imaging Spectrometer (AVIRIS) by NASA's Jet Propulsion Lab, Airborne Imaging Spectrometer Multispectral by Spectral Imaging, and Hyperspectral Digital Imagery Collection Experiment by the Naval Research Lab. Hyperspectral images can aid to eliminate both the potential limitations of low spatial and spectral resolutions and the limitations of discrete spectral signatures associated with other images. Hyperspectral sensors can simultaneously collect narrower and contiguous images with up to 200 spectral bands, which enable measurement and monitoring of WQPs.

Improvement in methods of analysis: Analysis and interpretation of WQPs using RS data should involve machine learning (ML) approaches instead of simple linear regressions as outlined for the retrieval of WQPs in Section 2.3.5. Although empirical methods of retrieval of WQPs are easy to implement and require less computation time and effort, they may not be effective in distinguishing some WQPs. ML models such as PCA, ANN, and SVM models, which have the potential to detect complicated nonlinear relationships through training and testing to improve the accuracy of WQP retrieved through RS, should be used.

Utilization of free and low-cost satellite images with fine spatial resolution: Although high resolution and hyperspectral images have high capabilities in discriminating WQPs, some of them come with a cost and may defeat the purpose of utilizing RS in water quality monitoring. Therefore, it is recommended that researchers should utilize Landsat images in the areas of water quality assessment. Landsat images have proven to be useful for small inland water systems including lakes, owing to their high spatial resolution (30 m) compared to coarse resolution images such as MODIS (250 m–1.1 km), MERIS (300 m), and SeaWiFS (1.1 km), which are more useful for coastal studies. Comparing Landsat programs to sensors of higher resolution such as those aboard the SPOT satellite program, ASTER, or IKONOS still places Landsat programs at an advantage owing to their more extensive long-term records dating back as far as the 1970s. The Landsat program is an open source with a highly accessible global spatial coverage data repository.

Author Contributions: Conceptualization, G.E.A., H.S. and S.A.; methodology, G.E.A.; writing—original draft preparation, G.E.A.; writing—review and editing, H.S., D.J. and S.A.; supervision, H.S. and S.A. All authors have read and agreed to the published version of the manuscript.

Funding: This research received no external funding.

Data Availability Statement: This work relied on published materials and public platforms, which have been duly referenced.

Conflicts of Interest: The authors declare no conflict of interest.

References

1. Chen, X.; Liu, L.; Zhang, X.; Li, J.; Wang, S.; Liu, D.; Duan, H.; Song, K. An Assessment of Water Color for Inland Water in China Using a Landsat 8-Derived Forel-Ule Index and the Google Earth Engine Platform. *IEEE J. Sel. Top. Appl. Earth Obs. Remote Sens.* **2021**, *14*, 5773–5785. [CrossRef]
2. Hajigholizadeh, M.; Moncada, A.; Kent, S.; Melesse, A.M. Land–lake linkage and remote sensing application in water quality monitoring in lake okeechobee, florida, usa. *Land* **2021**, *10*, 147. [CrossRef]
3. Schaeffer, B.A.; Schaeffer, K.G.; Keith, D.; Lunetta, R.S.; Conmy, R.; Gould, R.W. Barriers to adopting satellite remote sensing for water quality management. *Int. J. Remote Sens.* **2013**, *34*, 7534–7544. [CrossRef]
4. Uudeberg, K.; Aavaste, A.; Kõks, K.-L.; Ansper, A.; Uusõue, M.; Kangro, K.; Ansko, I.; Ligi, M.; Toming, K.; Reinart, A. Optical Water Type Guided Approach to Estimate Optical Water Quality Parameters. *Remote Sens.* **2020**, *12*, 931. [CrossRef]
5. Yang, H.; Kong, J.; Hu, H.; Du, Y.; Gao, M.; Chen, F. A Review of Remote Sensing for Water Quality Retrieval: Progress and Challenges. *Remote Sens.* **2022**, *14*, 1770. [CrossRef]

6. McCarthy, M.J.; Colna, K.E.; El-Mezayen, M.M.; Laureano-Rosario, A.E.; Méndez-Lázaro, P.; Otis, D.B.; Toro-Farmer, G.; Vega-Rodriguez, M.; Muller-Karger, F.E. Satellite Remote Sensing for Coastal Management: A Review of Successful Applications. *Environ. Manag.* **2017**, *60*, 323–339. [CrossRef]
7. Allan, M.G.; Hamilton, D.P.; Hicks, B.J.; Brabyn, L. Landsat remote sensing of chlorophyll a concentrations in central North Island lakes of New Zealand. *Int. J. Remote Sens.* **2011**, *32*, 2037–2055. [CrossRef]
8. Gholizadeh, M.H.; Melesse, A.M.; Reddi, L. Spaceborne and airborne sensors in water quality assessment. *Int. J. Remote Sens.* **2016**, *37*, 3143–3180. [CrossRef]
9. Adjovu, G.E.; Stephen, H.; Ahmad, S. Monitoring of Total Dissolved Solids Using Remote Sensing Band Reflectance and Salinity Indices: A Case Study of the Imperial County Section, AZ-CA, of the Colorado River. *World Environ. Water Resour. Congr.* **2022**, *2022*, 1132. [CrossRef]
10. Pizani, F.M.C.; Maillard, P.; Ferreira, A.F.F.; De Amorim, C.C. Estimation of Water Quality in a Reservoir from Sentinel-2 MSI amd Landsat-8 OLI Sensors. *ISPRS Ann. Photogramm. Remote Sens. Spat. Inf. Sci.* **2020**, *V-3-2020*, 401–408. [CrossRef]
11. Zhou, Y.; Dong, J.; Xiao, X.; Xiao, T.; Yang, Z.; Zhao, G.; Zou, Z.; Qin, Y. Open surface water mapping algorithms: A comparison of water-related spectral indices and sensors. *Water* **2017**, *9*, 256. [CrossRef]
12. Zhou, B.; Shang, M.; Wang, G.; Zhang, S.; Feng, L.; Liu, X.; Wu, L.; Shan, K. Distinguishing two phenotypes of blooms using the normalised difference peak-valley index (NDPI) and Cyano-Chlorophyta index (CCI). *Sci. Total Environ.* **2018**, *628–629*, 848–857. [CrossRef] [PubMed]
13. Gallagher, L.C. Hyperspectral Remote Sensing of Suspended Minerals, Chlorophyll and Coloured Dissolved Organic Matter in Coastal and Inland Waters, British Columbia, Canada. Mater's Thesis, University of Victoria, Victoria, BC, Canada, 2004.
14. Abbas, A.; Khan, S. Using remote sensing techniques for appraisal of irrigated soil salinity. In Land, Water Environment Management Integrated Systems for Sustainability, Proceedings of the MODSIM 2007 International Congress on Modelling and Simulation, Canberra, Australia, 10–13 December 2007; Modelling and Simulation Society of Australia and New Zealand: Christchurch, New Zealand, 2007; pp. 2632–2638.
15. Deutsch, E.S.; Alameddine, I.; El-Fadel, M. Monitoring water quality in a hypereutrophic reservoir using Landsat ETM+ and OLI sensors: How transferable are the water quality algorithms? *Environ. Monit. Assess.* **2018**, *190*, 141. [CrossRef]
16. Gholizadeh, M.H.; Melesse, A.M.; Reddi, L. A comprehensive review on water quality parameters estimation using remote sensing techniques. *Sensors* **2016**, *16*, 1298. [CrossRef] [PubMed]
17. Usali, N.; Ismail, M.H. Use of Remote Sensing and GIS in Monitoring Water Quality. *J. Sustain. Dev.* **2010**, *3*, 228–238. [CrossRef]
18. Dube, T.; Mutanga, O.; Seutloali, K.; Adelabu, S.; Shoko, C. Water quality monitoring in sub-Saharan African lakes: A review of remote sensing applications. *Afr. J. Aquat. Sci.* **2015**, *40*, 1–7. [CrossRef]
19. Avdan, Z.Y.; Kaplan, G.; Goncu, S.; Avdan, U. Monitoring the water quality of small water bodies using high-resolution remote sensing data. *ISPRS Int. J. Geo-Inf.* **2019**, *8*, 553. [CrossRef]
20. Olmanson, L.G.; Brezonik, P.L.; Bauer, M.E. Evaluation of medium to low resolution satellite imagery for regional lake water quality assessments. *Water Resour. Res.* **2011**, *47*, W09515. [CrossRef]
21. Alparslan, E.; Aydöner, C.; Tufekci, V.; Tüfekci, H. Water quality assessment at Ömerli Dam using remote sensing techniques. *Environ. Monit. Assess.* **2007**, *135*, 391–398. [CrossRef]
22. D'Ortenzio, F.; Marullo, S.; Ragni, M.; D'Alcalà, M.R.; Santoleri, R. Validation of empirical SeaWiFS algorithms for chlorophyll-a retrieval in the Mediterranean Sea: A case study for oligotrophic seas. *Remote Sens. Environ.* **2002**, *82*, 79–94. [CrossRef]
23. Gitelson, A.A.; Dall'Olmo, G.; Moses, W.; Rundquist, D.C.; Barrow, T.; Fisher, T.R.; Gurlin, D.; Holz, J. A simple semi-analytical model for remote estimation of chlorophyll-a in turbid waters: Validation. *Remote Sens. Environ.* **2008**, *112*, 3582–3593. [CrossRef]
24. He, W.; Chen, S.; Liu, X.; Chen, J. Water quality monitoring in a slightly-polluted inland water body through remote sensing—Case study of the Guanting Reservoir in Beijing, China. *Front. Environ. Sci. Eng. China* **2008**, *2*, 163–171. [CrossRef]
25. Isidro, C.M.; McIntyre, N.; Lechner, A.M.; Callow, I. Quantifying suspended solids in small rivers using satellite data. *Sci. Total Environ.* **2018**, *634*, 1554–1562. [CrossRef] [PubMed]
26. Karami, J.; Alimohammadi, A.; Modabberi, S. Analysis of the spatio-temporal patterns of water pollution and source contribution using the MODIS sensor products and multivariate statistical techniques. *IEEE J. Sel. Top. Appl. Earth Obs. Remote Sens.* **2012**, *5*, 1243–1255. [CrossRef]
27. Mabwoga, S.O.; Chawla, A.; Thukral, A.K. Assessment of water quality parameters of the Harike wetland in India, a Ramsar site, using IRS LISS IV satellite data. *Environ. Monit. Assess.* **2010**, *170*, 117–128. [CrossRef]
28. Maliki, A.A.A.; Chabuk, A.; Sultan, M.A.; Hashim, B.M.; Hussain, H.M.; Al-Ansari, N. Estimation of Total Dissolved Solids in Water Bodies by Spectral Indices Case Study: Shatt al-Arab River. *Water Air Soil Pollut.* **2020**, *231*, 482. [CrossRef]
29. Morel, A.; Bélanger, S. Improved detection of turbid waters from ocean color sensors information. *Remote Sens. Environ.* **2006**, *102*, 237–249. [CrossRef]
30. Pereira, O.J.R.; Merino, E.R.; Montes, C.R.; Barbiero, L.; Rezende-Filho, A.T.; Lucas, Y.; Melfi, A.J. Estimating water pH using cloud-based landsat images for a new classification of the Nhecolândia Lakes (Brazilian Pantanal). *Remote Sens.* **2020**, *12*, 1090. [CrossRef]
31. Petus, C.; Chust, G.; Gohin, F.; Doxaran, D.; Froidefond, J.M.; Sagarminaga, Y. Estimating turbidity and total suspended matter in the Adour River plume (South Bay of Biscay) using MODIS 250-m imagery. *Cont. Shelf Res.* **2010**, *30*, 379–392. [CrossRef]

32. Toming, K.; Kutser, T.; Tuvikene, L.; Viik, M.; Nõges, T. Dissolved organic carbon and its potential predictors in eutrophic lakes. *Water Res.* **2016**, *102*, 32–40. [CrossRef]
33. Ansper, A.; Alikas, K. Retrieval of chlorophyll a from Sentinel-2 MSI data for the European Union water framework directive reporting purposes. *Remote Sens.* **2019**, *11*, 64. [CrossRef]
34. Gómez, J.A.D.; Alonso, C.A.; García, A.A. Remote sensing as a tool for monitoring water quality parameters for Mediterranean Lakes of European Union water framework directive (WFD) and as a system of surveillance of cyanobacterial harmful algae blooms (SCyanoHABs). *Environ. Monit. Assess.* **2011**, *181*, 317–334. [CrossRef] [PubMed]
35. Potes, M.; Costa, M.J.; Salgado, R. Satellite remote sensing of water turbidity in Alqueva reservoir and implications on lake modelling. *Hydrol. Earth Syst. Sci.* **2012**, *16*, 1623–1633. [CrossRef]
36. Adjovu, G.E.; Ahmad, S.; Stephen, H. Analysis of Suspended Material in Lake Mead Using Remote Sensing Indices. *World Environ. Water Resour. Congr.* **2021**, *2021*, 754–768. [CrossRef]
37. Dekker, A.G.; Hestir, E.L. *Evaluating the Feasibility of Systematic Inland Water Quality Monitoring with Satellite Remote Sensing*; Water for a Healthy Country WIRADA; CSIRO: Canberra, Australia, 2012; p. 105.
38. AL-Fahdawi, A.A.H.; Rabee, A.M.; Al-Hirmizy, S.M. Water quality monitoring of Al-Habbaniyah Lake using remote sensing and in situ measurements. *Environ. Monit. Assess.* **2015**, *187*, 367. [CrossRef] [PubMed]
39. Karagiannis, I.C.; Soldatos, P.G. Water desalination cost literature: Review and assessment. *Desalination* **2008**, *223*, 448–456. [CrossRef]
40. Dey, J.; Vijay, R. A critical and intensive review on assessment of water quality parameters through geospatial techniques. *Environ. Sci. Pollut. Res.* **2021**, *28*, 41612–41626. [CrossRef]
41. Dörnhöfer, K.; Oppelt, N. Remote sensing for lake research and monitoring—Recent advances. *Ecol. Indic.* **2016**, *64*, 105–122. [CrossRef]
42. Karaoui, I.; Arioua, A.; Boudhar, A.; Hssaisoune, M.; El Mouatassime, S.; Ouhamchich, K.A.; Elhamdouni, D.; Idrissi, A.E.A.; Nouaim, W. Evaluating the potential of Sentinel-2 satellite images for water quality characterization of artificial reservoirs: The Bin El Ouidane Reservoir case study (Morocco). *Meteorol. Hydrol. Water Manag.* **2019**, *7*, 31–39.
43. Nath, R.K.; Deb, S.K. Water-Body Area Extraction From High Resolution Satellite Images-An Introduction, Review, and Comparison. *Int. J. Image Process.* **2010**, *3*, 353–372.
44. Palmer, S.C.J.; Kutser, T.; Hunter, P.D. Remote sensing of inland waters: Challenges, progress and future directions. *Remote Sens. Environ.* **2015**, *157*, 1–8. [CrossRef]
45. Song, K. Water quality monitoring using Landsat Themate Mapper data with empirical algorithms in Chagan Lake, China. *J. Appl. Remote Sens.* **2011**, *5*, 053506. [CrossRef]
46. Buma, W.G.; Lee, S.I. Evaluation of Sentinel-2 and Landsat 8 images for estimating Chlorophyll-a concentrations in Lake Chad, Africa. *Remote Sens.* **2020**, *12*, 2437. [CrossRef]
47. Ogashawara, I.; Mishra, D.R.; Gitelson, A.A. *Remote Sensing of Inland Waters: Background and Current State-of-the-Art*; Elsevier Inc.: Amsterdam, The Netherlands, 2017. [CrossRef]
48. Vakili, T.; Amanollahi, J. Determination of optically inactive water quality variables using Landsat 8 data: A case study in Geshlagh reservoir affected by agricultural land use. *J. Clean. Prod.* **2020**, *247*, 119134. [CrossRef]
49. Zhang, K.; Amineh, R.K.; Dong, Z.; Nadler, D. Microwave Sensing of Water Quality. *IEEE Access* **2019**, *7*, 69481–69493. [CrossRef]
50. Salmaso, N.; Mosello, R. Limnological research in the deep southern subalpine lakes: Synthesis, directions and perspectives. *Adv. Oceanogr. Limnol.* **2010**, *1*, 29–66. [CrossRef]
51. De Vlaming, V.; DiGiorgio, C.; Fong, S.; Deanovic, L.; Carpio-Obeso, M.D.L.P.; Miller, J.; Miller, M.; Richard, N. Irrigation runoff insecticide pollution of rivers in the Imperial Valley, California (USA). *Environ. Pollut.* **2004**, *132*, 213–229. [CrossRef]
52. Kimbrough, R.A.; Litke, D.W. Pesticides in streams draining agricultural and urban areas in Colorado. *Environ. Sci. Technol.* **1996**, *30*, 908–916. [CrossRef]
53. Stout, W.L.; Fales, S.L.; Muller, L.D.; Schnabel, R.R.; Elwinger, G.F.; Weaver, S.R. Assessing the effect of management intensive grazing on water quality in the northeast U.S. *J. Soil Water Conserv.* **2000**, *55*, 238–243.
54. Schliemann, S.A.; Grevstad, N.; Brazeau, R.H. Water quality and spatio-temporal hot spots in an effluent-dominated urban river. *Hydrol. Process.* **2021**, *35*, e14001. [CrossRef]
55. Masocha, M.; Murwira, A.; Magadza, C.H.D.; Hirji, R.; Dube, T. Remote sensing of surface water quality in relation to catchment condition in Zimbabwe. *Phys. Chem. Earth* **2017**, *100*, 13–18. [CrossRef]
56. Mueller, J.S.; Grabowski, T.B.; Brewer, S.K.; Worthington, T.A. Effects of temperature, total dissolved solids, and total suspended solids on survival and development rate of larval Arkansas River shiner. *J. Fish Wildl. Manag.* **2017**, *8*, 79–88. [CrossRef]
57. Fant, C.; Srinivasan, R.; Boehlert, B.; Rennels, L.; Chapra, S.C.; Strzepek, K.M.; Corona, J.; Allen, A.; Martinich, J. Climate change impacts on us water quality using two models: HAWQS and US basins. *Water* **2017**, *9*, 118. [CrossRef]
58. Tran, P.H.; Nguyen, A.K.; Liou, Y.-A.; Hoang, P.P.; Thanh, H.N. Estimation of Salinity Intrusion by Using Landsat 8 OLI Data in The Mekong Delta, Vietnam. *Prog. Earth Planet. Sci.* **2020**, *7*, 1. [CrossRef]
59. Hannah, D.M.; Brown, L.E.E.E.; Milner, A.M. Integrating climate—Hydrology—Ecology for alpine river systems. *Aquat. Conserv. Mar. Freshw. Ecosyst.* **2007**, *656*, 636–656. [CrossRef]

60. Gunatilaka, A.; Moscetta, P.; Sanfilippo, L. Recent Advancements in Water Quality Monitoring-the use of miniaturized sensors and novel analytical measuring techniques for in-situ and on-line real time. In Proceedings of the International Workshop on Monitoring and Sensor for Water Pollution Control, Beijing, China, 13–14 June 2007; pp. 33–43.
61. Oun, A.; Kumar, A.; Harrigan, T.; Angelakis, A.; Xagoraraki, I. Effects of biosolids and manure application on microbial water quality in rural areas in the US. *Water* **2014**, *6*, 3701–3723. [CrossRef]
62. Fujioka, R.S.; Solo-Gabriele, H.M.; Byappanahalli, M.N.; Kirs, M. U.S. recreational water quality criteria: A vision for the future. *Int. J. Environ. Res. Public Health* **2015**, *12*, 7752–7776. [CrossRef]
63. Vedwan, N.; Ahmad, S.; Miralles-Wilhelm, F.; Broad, K.; Letson, D.; Podesta, G. Institutional evolution in Lake Okeechobee Management in Florida: Characteristics, impacts, and limitations. *Water Resour. Manag.* **2008**, *22*, 699–718. [CrossRef]
64. Lee, S.; Ahn, K.H. Monitoring of COD as an organic indicator in waste water and treated effluent by fluorescence excitation-emission (FEEM) matrix characterization. *Water Sci. Technol.* **2004**, *50*, 57–63. [CrossRef]
65. El Serafy, G.Y.H.; Schaeffer, B.A.; Neely, M.-B.; Spinosa, A.; Odermatt, D.; Weathers, K.C.; Baracchini, T.; Bouffard, D.; Carvalho, L.; Conmy, R.N.; et al. Integrating Inland and Coastal Water Quality Data for Actionable Knowledge. *Remote Sens.* **2021**, *13*, 2899. [CrossRef]
66. Mondal, K.C.; Rathod, K.G.; Joshi, H.M.; Mandal, H.S.; Khan, R.; Rajendra, K.; Mawale, Y.K.; Priya, K.; Jhariya, D.C. Impact of land-use and land-cover change on groundwater quality and quantity in the Raipur, Chhattisgarh, India: A remote sensing and GIS approach. *IOP Conf. Ser. Earth Environ. Sci.* **2020**, *597*, 012011. [CrossRef]
67. Lin, W.; Li, Z. Detection and quantification of trace organic contaminants in water using the FT-IR-attenuated total reflectance technique. *Anal. Chem.* **2010**, *82*, 505–515. [CrossRef] [PubMed]
68. Tsuchiya, Y. Organical Chemicals As Contaminants of Water Bodies and Drinking Water. *Water Qual. Stand.* **2010**, *II*, 150–171.
69. Ibrahim, N.; Aziz, H.A. Trends on Natural Organic Matter in Drinking Water Sources and its Treatment. *Int. J. Sci. Res. Environ. Sci.* **2014**, *2*, 94–106. [CrossRef]
70. Christian, E.; Batista, J.R.; Gerrity, D. Use of COD, TOC, and Fluorescence Spectroscopy to Estimate BOD in Wastewater. *Water Environ. Res.* **2016**, *89*, 168–177. [CrossRef]
71. Hu, H.-Y.; Du, Y.; Wu, Q.Y.; Zhao, X.; Tang, X.; Chen, Z. Differences in dissolved organic matter between reclaimed water source and drinking water source. *Sci. Total Environ.* **2016**, *551–552*, 133–142. [CrossRef]
72. Cao, F.; Tzortziou, M.; Hu, C.; Mannino, A.; Fichot, C.G.; Del Vecchio, R.; Najjar, R.G.; Novak, M. Remote sensing retrievals of colored dissolved organic matter and dissolved organic carbon dynamics in North American estuaries and their margins. *Remote Sens. Environ.* **2018**, *205*, 151–165. [CrossRef]
73. Kutser, T.; Pierson, D.C.; Tranvik, L.; Reinart, A.; Sobek, S.; Kallio, K. Using satellite remote sensing to estimate the colored dissolved organic matter absorption coefficient in lakes. *Ecosystems* **2005**, *8*, 709–720. [CrossRef]
74. Al-Kharusi, E.S.; Tenenbaum, D.E.; Abdi, A.M.; Kutser, T.; Karlsson, J.; Bergström, A.-K.; Berggren, M. Large-Scale Retrieval of Coloured Dissolved Organic Matter in Northern Lakes Using Sentinel-2 Data. *Remote Sens.* **2020**, *12*, 157. [CrossRef]
75. Rieger, L.; Langergraber, G.; Thomann, M.; Fleischmann, N.; Siegrist, H. Spectral in-situ analysis of NO2, NO3, COD, DOC and TSS in the effluent of a WWTP. *Water Sci. Technol.* **2004**, *50*, 143–152. [CrossRef]
76. Cao, F.; Tzortziou, M. Capturing dissolved organic carbon dynamics with Landsat-8 and Sentinel-2 in tidally influenced wetland–estuarine systems. *Sci. Total Environ.* **2021**, *777*, 145910. [CrossRef]
77. Wei, K.L.; Chen, M.; Wang, F.; Fang, Q. A rapid monitoring system for the determination of COD in waters based on ultrasonic assisted digestion and miniaturized spectral analytical system. *Appl. Mech. Mater.* **2013**, *401–403*, 1295–1300. [CrossRef]
78. Denys, L. Incomplete spring turnover in small deep lakes in SE Michigan. *McNair Sch. Res. J.* **2010**, *2*, 133–144.
79. Hasab, H.A.; Jawad, H.A.; Dibs, H.; Hussain, H.M.; Al-Ansari, N. Evaluation of Water Quality Parameters in Marshes Zone Southern of Iraq Based on Remote Sensing and GIS Techniques. *Water. Air. Soil Pollut.* **2020**, *231*, 183. [CrossRef]
80. Fletcher, T.D.; Andrieu, H.; Hamel, P. Understanding, management and modelling of urban hydrology and its consequences for receiving waters: A state of the art. *Adv. Water Resour.* **2013**, *51*, 261–279. [CrossRef]
81. Bonansea, M.; Ledesma, M.; Rodriguez, C.; Pinotti, L. Using new remote sensing satellites for assessing water quality in a reservoir. *Hydrol. Sci. J.* **2019**, *64*, 34–44. [CrossRef]
82. Hidayati, N.F.; Rahman, M.; Fauzana, N.A.; Aisiah, S. Effectiveness of Chitosan To Reduce the Color Value, Turbidity, and Total Dissolved Solids in Shrimp-Washing Wastewater. *Russ. J. Agric. Socio-Econ. Sci.* **2021**, *115*, 82–88. [CrossRef]
83. Mehdinejad, M.H.; Bina, B.; Nikaeen, M.; Attar, H.M. Effectiveness of natural and synthetic polyelectrolytes as coagulant aid in removal of turbidity from different turbid waters. *J. Food Agric. Environ.* **2013**, *29*, 261–266.
84. Hellweger, F.L.; Schlosser, P.; Lall, U.; Weissel, J.K. Use of satellite imagery for water quality studies in New York Harbor. *Estuar. Coast. Shelf Sci.* **2004**, *61*, 437–448. [CrossRef]
85. Chen, Q.; Zhang, Y.; Hallikainen, M. Water quality monitoring using remote sensing in support of the EU water framework directive (WFD): A case study in the Gulf of Finland. *Environ. Monit. Assess.* **2007**, *124*, 157–166. [CrossRef]
86. Li, S.; Song, K.; Wang, S.; Liu, G.; Wen, Z.; Shang, Y.; Lyu, L.; Chen, F.; Xu, S.; Tao, H.; et al. Quantification of chlorophyll-a in typical lakes across China using Sentinel-2 MSI imagery with machine learning algorithm. *Sci. Total Environ.* **2021**, *778*, 146271. [CrossRef] [PubMed]

87. Wei, J.; Lee, Z.; Ondrusek, M.; Mannino, A.; Tzortziou, M.; Armstrong, R. Spectral slopes of the absorption coefficient of colored dissolved and detrital material inverted from UV-visible remote sensing reflectance. *J. Geophys. Res. Ocean.* **2016**, *121*, 3010–3028. [CrossRef] [PubMed]
88. Artlett, C.P.; Pask, H.M. New approach to remote sensing of temperature and salinity in natural water samples. *Opt. Express* **2017**, *25*, 2840. [CrossRef]
89. Hossain, A.K.M.A.; Mathias, C.; Blanton, R. Remote sensing of turbidity in the tennessee river using landsat 8 satellite. *Remote Sens.* **2021**, *13*, 3785. [CrossRef]
90. Li, R.; Li, J. Satellite Remote Sensing Technology for Lake Water Clarity Monitoring: An Overview. *Environ. Inform. Arch.* **2004**, *2*, 893–901.
91. Devlin, M.J.; Petus, C.; Da Silva, E.; Tracey, D.; Wolff, N.H.; Waterhouse, J.; Brodie, J. Water quality and river plume monitoring in the Great Barrier Reef: An overview of methods based on ocean colour satellite data. *Remote Sens.* **2015**, *7*, 12909–12941. [CrossRef]
92. Engman, E.T. Remote sensing in hydrology. *Geophys. Monogr. Ser.* **1998**, *108*, 165–177. [CrossRef]
93. Varotsos, C.A.; Krapivin, V.F. *Microwave Remote Sensing Tools in Environmental Science*; Springer: Cham, Switzerland, 2020. [CrossRef]
94. Quemada, C.; Pérez-Escudero, J.M.; Gonzalo, R.; Ederra, I.; Santesteban, L.G.; Torres, N.; Iriarte, J.C. Remote Sensing for Plant Water Content Monitoring: A Review. *Remote Sensing* **2021**, *13*, 2088. [CrossRef]
95. Sagan, V.; Peterson, K.T.; Maimaitijiang, M.; Sidike, P.; Sloan, J.; Greeling, B.A.; Maalouf, S.; Adams, C. Monitoring inland water quality using remote sensing: Potential and limitations of spectral indices, bio-optical simulations, machine learning, and cloud computing. *Earth-Sci. Rev.* **2020**, *205*, 103187. [CrossRef]
96. Zhou, X.; Liu, X.; Wang, X.; He, G.; Zhang, Y.; Wang, G.; Zhang, Z. Evaluation of surface reflectance products based on optimized 6s model using synchronous in situ measurements. *Remote Sens.* **2022**, *14*, 83. [CrossRef]
97. Bernier, P.Y. Microwave remote sensing of snowpack properties: Potential and limitations. *Nord. Hydrol.* **1987**, *18*, 1–20. [CrossRef]
98. Government of Canada. Microwave Remote Sensing Introduction. 2015. Available online: https://www.nrcan.gc.ca/maps-tools-and-publications/satellite-imagery-and-air-photos/tutorial-fundamentals-remote-sensing/microwave-remote-sensing/9371 (accessed on 10 February 2023).
99. Herndon, K.; Meyer, F.; Flores, A.; Cherrington, E.; Kucera, L. What is Synthetic Aperture Radar? Earthdata. NASA Earthdata. Available online: https://www.earthdata.nasa.gov/learn/backgrounders/what-is-sar (accessed on 10 February 2023).
100. Carter, W.D.; Engman, E.T. *Remote Sensing from Satellites*; Elsevier Inc.: Amsterdam, The Netherlands, 1984. [CrossRef]
101. Kumar, D.N.; Reshmidevi, T.V. Remote sensing applications in water resources. *J. Indian Inst. Sci.* **2013**, *93*, 163–188.
102. Mishra, A.K. Understanding Non-optical Remote-sensed Images: Needs, Challenges and Ways Forward. *arXiv* **2016**, arXiv:1612.07921.http://arxiv.org/abs/1612.07921.
103. Terentev, A.; Dolzhenko, V.; Fedotov, A.; Eremenko, D. Current State of Hyperspectral Remote Sensing for Early Plant Disease Detection: A Review. *Sensors* **2022**, *22*, 757. [CrossRef]
104. Tsang, L.; Liao, T.-H.; Gao, R.; Xu, H.; Gu, W.; Zhu, J. Theory of Microwave Remote Sensing of Vegetation Effects, SoOp and Rough Soil Surface Backscattering. *Remote Sens.* **2022**, *14*, 3640. [CrossRef]
105. Klein, M.E.; Aalderink, B.J.; Padoan, R.; De Bruin, G.; Steemers, T.A.G. Quantitative hyperspectral reflectance imaging. *Sensors* **2008**, *8*, 5576–5618. [CrossRef] [PubMed]
106. Matthews, M.W.; Bernard, S.; Evers-King, H.; Lain, L.R. Distinguishing cyanobacteria from algae in optically complex inland waters using a hyperspectral radiative transfer inversion algorithm. *Remote Sens. Environ.* **2020**, *248*, 111981. [CrossRef]
107. Allbed, A.; Kumar, L. Soil Salinity Mapping and Monitoring in Arid and Semi-Arid Regions Using Remote Sensing Technology: A Review. *Adv. Remote Sens.* **2013**, *02*, 373–385. [CrossRef]
108. Govender, M.; Chetty, K.; Bulcock, H. A review of hyperspectral remote sensing and its application in vegetation and water resource studies. *Water SA* **2007**, *33*, 145–151. [CrossRef]
109. Lyu, S.; Huang, C.; Hou, M. Reflectance reconstruction of hyperspectral image based on gaussian surface fitting. *Int. Arch. Photogramm. Remote Sens. Spat. Inf. Sci.—ISPRS Arch.* **2020**, *43*, 1365–1369. [CrossRef]
110. Fan, C. Spectral Analysis of Water Reflectance for Hyperspectral Remote Sensing of Water Quailty in Estuarine Water. *J. Geosci. Environ. Prot.* **2014**, *2*, 19–27. [CrossRef]
111. Jay, S.; Guillaume, M. Regularized estimation of bathymetry and water quality using hyperspectral remote sensing. *Int. J. Remote Sens.* **2016**, *37*, 263–289. [CrossRef]
112. Topp, S.N.; Pavelsky, T.M.; Jensen, D.; Simard, M.; Ross, M.R.V. Research trends in the use of remote sensing for inland water quality science: Moving towards multidisciplinary applications. *Water* **2020**, *12*, 169. [CrossRef]
113. ESA. Sentinel Resolutionand Swath. pp. 1–2. Available online: https://sentinels.copernicus.eu/web/sentinel/missions/sentinel-2/instrument-payload/resolution-and-swath (accessed on 10 February 2023).
114. Normand, A.E. Landsat 9 and the Future of the Sustainable Land Imaging Program. 2020; p. 31. Available online: https://crsreports.congress.gov/product/pdf/R/R46560 (accessed on 10 February 2023).
115. Li, J.; Roy, D.P. A global analysis of Sentinel-2a, Sentinel-2b and Landsat-8 data revisit intervals and implications for terrestrial monitoring. *Remote Sens.* **2017**, *9*, 902. [CrossRef]

116. USGS. Landsat 8. Available online: https://www.usgs.gov/landsat-missions/landsat-8?qt-science_support_page_related_con=0 (accessed on 10 February 2023).
117. Sayler, K. Landsat 9 Data Users Handbook Landsat 9 Data Users Handbook Version 1.0. no. February 2022; p. 107. Available online: https://d9-wret.s3.us-west-2.amazonaws.com/assets/palladium/production/s3fs-public/media/files/LSDS-2082_L9-Data-Users-Handbook_v1.pdf (accessed on 10 February 2023).
118. USGS. What Are the Acquisition Schedules for the Landsat Satellites? Available online: https://www.usgs.gov/faqs/what-are-acquisition-schedules-landsat-satellites#:~:text=Eachsatellitemakesacomplete,sceneareaontheglobe (accessed on 10 February 2023).
119. USGS. Landsat 7. NASA Landsat Science. Available online: https://landsat.gsfc.nasa.gov/satellites/landsat-7/ (accessed on 10 February 2023).
120. Chander, G.; Markham, B.L.; Helder, D.L. Summary of current radiometric calibration coefficients for Landsat MSS, TM, ETM+, and EO-1 ALI sensors. *Remote Sens. Environ.* **2009**, *113*, 893–903. [CrossRef]
121. Allan, M.G.; Hicks, B.J.; Brabyn, L. *Remote Sensing of Water Quality in the Rotorua Lakes*; University of Waikato: Hamilton, New Zealand, 2007.
122. Chander, G.; Markham, B.L.; Barsi, J.A. Revised landsat-5 thematic mapper radiometric calibration. *IEEE Geosci. Remote Sens. Lett.* **2007**, *4*, 490–494. [CrossRef]
123. USGS. Landsat 5. USGS Website. Available online: https://www.usgs.gov/landsat-missions/landsat-8 (accessed on 2 April 2023).
124. SEOS. Introduction to remote sensing Resolution. Available online: https://seos-project.eu/remotesensing/remotesensing-c03-p01.html (accessed on 10 February 2023).
125. Abrams, M.; Hook, S.; Ramachandran, B. ASTER User Handbook. Jet Propulsion Laboratory: Pasadena, CA, USA; EROS Data Center: Sioux Falls, SD, USA, 2002.
126. Kumar, N.; Chu, A.D.; Foster, A.D.; Peters, T.; Willis, R. Satellite Remote Sensing for Developing Time and Space Resolved Estimates of Ambient Particulate in Cleveland, OH. *Aerosol Sci. Technol.* **2013**, *18*, 1199–1216. [CrossRef]
127. NASA. Terra & Aqua Moderate Resolution Imaging Spectroradiometer (MODIS). Available online: https://ladsweb.modaps.eosdis.nasa.gov/missions-and-measurements/modis/ (accessed on 10 February 2023).
128. Hu, C.; Chen, Z.; Clayton, T.D.; Swarzenski, P.; Brock, J.C.; Muller-Karger, F.E. Assessment of estuarine water-quality indicators using MODIS medium-resolution bands: Initial results from Tampa Bay, FL. *Remote Sens. Environ.* **2004**, *93*, 423–441. [CrossRef]
129. Phiri, D.; Simwanda, M.; Salekin, S.; Nyirenda, V.R.; Murayama, Y.; Ranagalage, M. Sentinel-2 data for land cover/use mapping: A review. *Remote Sens.* **2020**, *12*, 2291. [CrossRef]
130. European Space Agency. About Copernicus Sentinel-2. 2020, p. 1. Available online: https://sentinels.copernicus.eu/web/sentinel/missions/sentinel-2/overview (accessed on 10 February 2023).
131. Shrestha, B.; Stephen, H.; Ahmad, S. Impervious surfaces mapping at city scale by fusion of radar and optical data through a random forest classifier. *Remote Sens.* **2021**, *13*, 3040. [CrossRef]
132. ESA. Sentinel Orbit. Available online: https://sentinels.copernicus.eu/web/sentinel/missions/sentinel-2/satellite-description/orbit (accessed on 10 February 2023).
133. Shrestha, B.; Ahmad, S.; Stephen, H. Fusion of Sentinel-1 and Sentinel-2 data in mapping the impervious surfaces at city scale. *Environ. Monit. Assess.* **2021**, *193*, 556. [CrossRef] [PubMed]
134. ESA. Sentinel-2. Available online: https://sentinel.esa.int/web/sentinel/missions/sentinel-2 (accessed on 10 February 2023).
135. Chawla, I.; Karthikeyan, L.; Mishra, A.K. A review of remote sensing applications for water security: Quantity, quality, and extremes. *J. Hydrol.* **2020**, *585*, 124826. [CrossRef]
136. ESA. ERS SAR Applications. Available online: https://earth.esa.int/eogateway/instruments/sar-ers/description (accessed on 10 February 2023).
137. Mohseni, F.; Saba, F.; Mirmazloumi, S.M.; Amani, M.; Mokhtarzade, M.; Jamali, S.; Mahdavi, S. Ocean water quality monitoring using remote sensing techniques: A review. *Mar. Environ. Res.* **2022**, *180*, 105701. [CrossRef] [PubMed]
138. Guo, H.; Huang, J.J.; Chen, B.; Guo, X.; Singh, V.P. A machine learning-based strategy for estimating non-optically active water quality parameters using Sentinel-2 imagery. *Int. J. Remote Sens.* **2021**, *42*, 1841–1866. [CrossRef]
139. Ávila, D.M.; Torres-Bejarano, F.; Lara, Z.M. Spectral indices for estimating total dissolved solids in freshwater wetlands using semi-empirical models. A case study of Guartinaja and Momil wetlands. *Int. J. Remote Sens.* **2022**, *43*, 2156–2184. [CrossRef]
140. Odermatt, D.; Gitelson, A.; Brando, V.E.; Schaepman, M. Review of constituent retrieval in optically deep and complex waters from satellite imagery. *Remote Sens. Environ.* **2012**, *118*, 116–126. [CrossRef]
141. Moore, G.K. Satellite remote sensing of water turbidity. *Hydrol. Sci. Bull.* **1980**, *25*, 407–421. [CrossRef]
142. Giardino, C.; Bresciani, M.; Braga, F.; Cazzaniga, I.; De Keukelaere, L.; Knaeps, E.; Brando, V.E. Chapter 5—Bio-optical Modeling of Total Suspended Solids. In *Bio-Optical Modeling of Total Suspended Solids*; Elsevier Inc.: Amsterdam, The Netherlands, 2017. [CrossRef]
143. Tzortziou, M.; Herman, J.R.; Gallegos, C.L.; Neale, P.J.; Subramaniam, A.; Harding, L.W.; Ahmad, Z. Bio-Optics of the Chesapeake Bay from Measurements and Radiative Transfer Closure. *Estuar. Coast. Shelf Sci.* **2006**, *68*, 348–362. [CrossRef]
144. Dekker, A.G.; Zamurovic, Ž.; Hoogenboom, H.J.; Peters, S.W.M. Remote sensing, ecological water quality modelling and in situ measurements: A case study in shallow lakes. *Hydrol. Sci. J.* **1996**, *41*, 531–547. [CrossRef]

145. Al, A.E. Landsat data to estimate a model of water quality parameters in Tigris and Euphrates rivers—Iraq. *Int. J. Adv. Appl. Sci.* **2019**, *6*, 50–58. [CrossRef]
146. Zhang, Y.; Pulliainen, J.; Koponen, S.; Hallikainen, M. Application of an empirical neural network to surface water quality estimation in the Gulf of Finland using combined optical data and microwave data. *Remote Sens. Environ.* **2002**, *81*, 327–336. [CrossRef]
147. Nima, C.; Frette, Ø.; Hamre, B.; Stamnes, J.J.; Chen, Y.-C.; Sørensen, K.; Norli, M.; Lu, D.; Xing, Q.; Muyimbwa, D.; et al. CDOM Absorption Properties of Natural Water Bodies along Extreme Environmental Gradients. *Water* **2019**, *11*, 1988. [CrossRef]
148. Ondrusek, M.; Stengel, E.; Kinkade, C.; Vogel, R.; Keegstra, P.; Hunter, C.; Kim, C. The development of a new optical total suspended matter algorithm for the Chesapeake Bay. *Remote Sens. Environ.* **2012**, *119*, 243–254. [CrossRef]
149. Herrault, P.A.; Gandois, L.; Gascoin, S.; Tananaev, N.; Le Dantec, T.; Teisserenc, R. Using high spatio-temporal optical remote sensing to monitor dissolved organic carbon in the Arctic river Yenisei. *Remote Sens.* **2016**, *8*, 803. [CrossRef]
150. Novoa, S.; Doxaran, D.; Ody, A.; Vanhellemont, Q.; Lafon, V.; Lubac, B.; Gernez, P. Atmospheric corrections and multi-conditional algorithm for multi-sensor remote sensing of suspended particulate matter in low-to-high turbidity levels coastal waters. *Remote Sens.* **2017**, *9*, 61. [CrossRef]
151. Giardino, C.; Bresciani, M.; Cazzaniga, I.; Schenk, K.; Rieger, P.; Braga, F.; Matta, E.; Brando, V.E. Evaluation of multi-resolution satellite sensors for assessing water quality and bottom depth of Lake Garda. *Sensors* **2014**, *14*, 24116–24131. [CrossRef]
152. Allan, M.G.; Hamilton, D.P.; Hicks, B.; Brabyn, L. Empirical and semi-analytical chlorophyll a algorithms for multi-temporal monitoring of New Zealand lakes using Landsat. *Environ. Monit. Assess.* **2015**, *187*, 364. [CrossRef]
153. Ansari, M.; Akhoondzadeh, M. Mapping water salinity using Landsat-8 OLI satellite images (Case study: Karun basin located in Iran). *Adv. Space Res.* **2020**, *65*, 1490–1502. [CrossRef]
154. Dinnat, E.P.; Le Vine, D.M.; Boutin, J.; Meissner, T.; Lagerloef, G. Remote sensing of sea surface salinity: Comparison of satellite and in situ observations and impact of retrieval parameters. *Remote Sens.* **2019**, *11*, 750. [CrossRef]
155. Kim, H.C.; Son, S.; Kim, Y.H.; Khim, J.S.; Nam, J.; Chang, W.K.; Lee, J.-H.; Lee, C.-H.; Ryu, J. Remote sensing and water quality indicators in the Korean West coast: Spatio-temporal structures of MODIS-derived chlorophyll-a and total suspended solids. *Mar. Pollut. Bull.* **2017**, *121*, 425–434. [CrossRef]
156. Le Vine, D.M.; Dinnat, E.P. The multifrequency future for remote sensing of sea surface salinity from space. *Remote Sens.* **2020**, *12*, 1381. [CrossRef]
157. Nguyen, P.T.B.; Koedsin, W.; McNeil, D.; Van, T.P.D. Remote sensing techniques to predict salinity intrusion: Application for a data-poor area of the coastal Mekong Delta, Vietnam. *Int. J. Remote Sens.* **2018**, *39*, 6676–6691. [CrossRef]
158. Pahlevan, N.; Chittimalli, S.K.; Balasubramanian, S.V.; Vellucci, V. Sentinel-2/Landsat-8 product consistency and implications for monitoring aquatic systems. *Remote Sens. Environ.* **2019**, *220*, 19–29. [CrossRef]
159. Poddar, S.; Chacko, N.; Swain, D. Estimation of Chlorophyll-a in Northern Coastal Bay of Bengal Using Landsat-8 OLI and Sentinel-2 MSI Sensors. *Front. Mar. Sci.* **2019**, *6*, 598. [CrossRef]
160. Sanjoto, T.B.; Elwafa, A.H.; Tjahjono, H.; Sidiq, W.A.B.N. Study of total suspended solid concentration based on Doxaran algorithm using Landsat 8 image in coastal water between Bodri River estuary up to east flood canal Semarang City. *IOP Conf. Ser. Earth Environ. Sci.* **2020**, *561*, 012053. [CrossRef]
161. Sun, D.; Su, X.; Qiu, Z.; Wang, S.; Mao, Z.; He, Y. Remote sensing estimation of sea surface salinity from GOCI measurements in the southern Yellow Sea. *Remote Sens.* **2019**, *11*, 775. [CrossRef]
162. Batur, E.; Maktav, D. Assessment of Surface Water Quality by Using Satellite Images Fusion Based on PCA Method in the Lake Gala, Turkey. *IEEE Trans. Geosci. Remote Sens.* **2019**, *57*, 2983–2989. [CrossRef]
163. Liu, J.; Hirose, T.; Kapfer, M.; Bennett, J.; McCullough, G.; Hocheim, K.; Stainton, M. Operational water quality monitoring over Lake Winnipeg using satellite remote sensing data. In Proceedings of the American Society for Photogrammetry and Remote Sensing-28th Canadian Symposium on Remote Sensing and ASPRS Fall Specialty Conference, Ottawa, ON, Canada, 28 October–1 November 2007; Volume 2007, pp. 151–160.
164. Rokni, K.; Ahmad, A.; Selamat, A.; Hazini, S. Water feature extraction and change detection using multitemporal landsat imagery. *Remote Sens.* **2014**, *6*, 4173–4189. [CrossRef]
165. Khanal, S.; Kushal, K.C.; Fulton, J.P.; Shearer, S.; Ozkan, E. Remote sensing in agriculture—Accomplishments, limitations, and opportunities. *Remote Sens.* **2020**, *12*, 3783. [CrossRef]
166. Nunziata, F.; Li, X.; Marino, A.; Shao, W.; Portabella, M.; Yang, X.; Buono, A. Microwave satellite measurements for coastal area and extreme weather monitoring. *Remote Sens.* **2021**, *13*, 3126. [CrossRef]
167. Johnson, R.W.; Harriss, R.C. Remote sensing for water quality and biological measurements in coastal waters. *Photogramm. Eng. Remote Sens.* **1980**, *46*, 77–85.
168. Miller, R.L.; McKee, B.A. Using MODIS Terra 250 m imagery to map concentrations of total suspended matter in coastal waters. *Remote Sens. Environ.* **2004**, *93*, 259–266. [CrossRef]
169. Wang, C.; Li, W.; Chen, S.; Li, D.; Wang, D.; Liu, J. The spatial and temporal variation of total suspended solid concentration in Pearl River Estuary during 1987–2015 based on remote sensing. *Sci. Total Environ.* **2018**, *618*, 1125–1138. [CrossRef] [PubMed]
170. Chen, J.; Quan, W.; Cui, T.; Song, Q. Estimation of total suspended matter concentration from MODIS data using a neural network model in the China eastern coastal zone. *Estuar. Coast. Shelf Sci.* **2015**, *155*, 104–113. [CrossRef]

171. Bhatti, A.M.; Rundquist, D.C.; Nasu, S.; Takagi, M. Assessing the potential of remotely sensed data for water quality monitoring of coastal and inland waters. *Soc. Soc. Manag. Syst.* **2008**, 1–7.
172. Sudheer, K.P.; Chaubey, I.; Garg, V. Lake water quality assessment from landsat thematic mapper data using neural network: An approach to optimal band combination selection. *J. Am. Water Resour. Assoc.* **2006**, *42*, 1683–1695. [CrossRef]
173. Hamidi, S.A.; Hosseiny, H.; Ekhtari, N.; Khazaei, B. Using MODIS remote sensing data for mapping the spatio-temporal variability of water quality and river turbid plume. *J. Coast. Conserv.* **2017**, *21*, 939–950. [CrossRef]
174. Azzam, A.; Uddin, H.; Mannan, U. Estimation of Suspended Sediment Concentration of Keenjhar Lake through Remote Sensing. *Eng. Proc.* **2022**, *22*, 20.
175. Lim, J.; Choi, M. Assessment of water quality based on Landsat 8 operational land imager associated with human activities in Korea. *Environ. Monit. Assess.* **2015**, *187*, 384. [CrossRef]
176. Song, K.; Li, L.; Li, S.; Tedesco, L.; Hall, B.; Li, L. Hyperspectral remote sensing of total phosphorus (TP) in three central Indiana water supply reservoirs. *Water. Air Soil Pollut.* **2012**, *223*, 1481–1502. [CrossRef]
177. Doxaran, D.; Cherukuru, R.C.N.; Lavender, S.J. Use of reflectance band ratios to estimate suspended and dissolved matter concentrations in estuarine waters. *Int. J. Remote Sens.* **2005**, *26*, 1763–1769. [CrossRef]
178. Saberioon, M.; Brom, J.; Nedbal, V.; Souc, P.; Císar, P. Chlorophyll-a and total suspended solids retrieval and mapping using Sentinel-2A and machine learning for inland waters. *Ecol. Indic.* **2020**, *113*, 106236. [CrossRef]
179. El Din, E.S.; Zhang, Y.; Suliman, A. Mapping concentrations of surface water quality parameters using a novel remote sensing and artificial intelligence framework. *Int. J. Remote Sens.* **2017**, *38*, 1023–1042. [CrossRef]
180. Giardino, C.; Bresciani, M.; Stroppiana, D.; Oggioni, A.; Morabito, G. Optical remote sensing of lakes: An overview on Lake Maggiore. *J. Limnol.* **2014**, *73*, 201–214. [CrossRef]
181. Somvanshi, S.; Kunwar, P.; Singh, N.B.; Shukla, S.P.; Pathak, V. Integrated remote sensing and GIS approach for water quality analysis of Gomti river, Uttar Pradesh. *Int. J. Environ. Sci.* **2012**, *3*, 62–75. [CrossRef]
182. Braga, F.; Giardino, C.; Bassani, C.; Matta, E.; Candiani, G.; Strömbeck, N.; Adamo, M.; Bresciani, M. Assessing water quality in the northern adriatic sea from hicotm data. *Remote Sens. Lett.* **2013**, *4*, 1028–1037. [CrossRef]
183. Giardino, C.; Brando, V.E.; Dekker, A.G.; Strömbeck, N.; Candiani, G. Assessment of water quality in Lake Garda (Italy) using Hyperion. *Remote Sens. Environ.* **2007**, *109*, 183–195. [CrossRef]
184. Alparslan, E.; Coskun, H.G.; Alganci, U. Water quality determination of Küçükçekmece Lake, Turkey by using multispectral satellite data. *Sci. World J.* **2009**, *9*, 1215–1229. [CrossRef]
185. Gitelson, A.A.; Gurlin, D.; Moses, W.J.; Barrow, T. A bio-optical algorithm for the remote estimation of the chlorophyll-a concentration in case 2 waters. *Environ. Res. Lett.* **2009**, *4*, 2–7. [CrossRef]
186. Moses, W.J.; Gitelson, A.A.; Berdnikov, S.; Povazhnyy, V. Satellite estimation of chlorophyll-a concentration using the red and NIR bands of MERISThe azov sea case study. *IEEE Geosci. Remote Sens. Lett.* **2009**, *6*, 845–849. [CrossRef]
187. Brezonik, P.; Menken, K.D.; Bauer, M. Landsat-based remote sensing of lake water quality characteristics, including chlorophyll and colored dissolved organic matter (CDOM). *Lake Reserv. Manag.* **2005**, *21*, 373–382. [CrossRef]
188. Chebud, Y.; Naja, G.M.; Rivero, R.G.; Melesse, A.M. Water quality monitoring using remote sensing and an artificial neural network. *Water Air Soil Pollut.* **2012**, *223*, 4875–4887. [CrossRef]
189. Osinska-Skotak, K.; Kruk, M.; Mróz, M. The Spatial Diversification of Lake Water Quality Parameters in Mazurian Lakes in Summertime. In *New Developments and Challenges in Remote Sensing*; Millpress: Rotterdam, The Netherlands, 2007; pp. 591–602.
190. Wu, M.; Zhang, W.; Wang, X.; Luo, D. Application of MODIS satellite data in monitoring water quality parameters of Chaohu Lake in China. *Environ. Monit. Assess.* **2009**, *148*, 255–264. [CrossRef] [PubMed]
191. Zhu, W.; Yu, Q.; Tian, Y.Q.; Chen, R.F.; Gardner, G.B. Estimation of chromophoric dissolved organic matter in the Mississippi and Atchafalaya river plume regions using above-surface hyperspectral remote sensing. *J. Geophys. Res. Ocean.* **2011**, *116*, C02011. [CrossRef]
192. Shirke, S.; Pinto, S.M.; Kushwaha, V.K.; Mardikar, T.; Vijay, R. Object-based image analysis for the impact of sewage pollution in Malad Creek, Mumbai, India. *Environ. Monit. Assess.* **2016**, *188*, 95. [CrossRef] [PubMed]
193. Álvarez-Robles, J.A.; Zarazaga-Soria, F.J.; Latre, M.Á.; Béjar, R.; Muro-Medrano, P.R. Water quality monitoring based on sediment distribution using satellite imagery. In Proceedings of the 2006—9th AGILE International Conference on Geographic Information Science "Shaping the Future of Geographic Information Science in Europe", Visegrád, Hungary, 20–22 April 2006; Volume 2006, pp. 144–150.
194. Vijay, R.; Pinto, S.M.; Kushwaha, V.K.; Pal, S.; Nandy, T. A multi-temporal analysis for change assessment and estimation of algal bloom in Sambhar Lake, Rajasthan, India. *Environ. Monit. Assess.* **2016**, *188*, 510. [CrossRef] [PubMed]
195. Mallick, J.; Hasan, M.A.; Alashker, Y.; Ahmed, M. Bathymetric and Geochemical Analysis of Lake Al-Saad, Abha, Kingdom of Saudi Arabia Using Geoinformatics Technology. *J. Geogr. Inf. Syst.* **2014**, *06*, 440–452. [CrossRef]
196. Li, Y.; Zhang, Y.; Shi, K.; Zhu, G.; Zhou, Y.; Zhang, Y.; Guo, Y. Monitoring spatiotemporal variations in nutrients in a large drinking water reservoir and their relationships with hydrological and meteorological conditions based on Landsat 8 imagery. *Sci. Total Environ.* **2017**, *599–600*, 1705–1717. [CrossRef]
197. Wu, C.; Wu, J.; Qi, J.; Zhang, L.; Huang, H.; Lou, L.; Chen, Y. Empirical estimation of total phosphorus concentration in the mainstream of the Qiantang River in China using Landsat TM data. *Int. J. Remote Sens.* **2010**, *31*, 2309–2324. [CrossRef]

198. Mustafa, M.T.; Hassoon, K.I.; Hussain, H.M.; Abd, M.H. Using Water Indices (Ndwi, Mndwi, Ndmi, Wri and Awei) To Detect Physical and Chemical Parameters By Apply Remote Sensing and Gis Techniques. *Int. J. Res.-Granthaalayah* **2017**, *5*, 117–128. [CrossRef]
199. Japitana, M.V.; Burce, M.E.C. A Satellite-based Remote Sensing Technique for Surface Water Quality Estimation. *Eng. Technol. Appl. Sci. Res.* **2019**, *9*, 3965–3970. [CrossRef]
200. Wang, Y.; Xia, H.; Fu, J.; Sheng, G. Water quality change in reservoirs of Shenzhen, China: Detection using LANDSAT/TM data. *Sci. Total Environ.* **2004**, *328*, 195–206. [CrossRef] [PubMed]
201. Yang, B.; Liu, Y.; Ou, F.; Yuan, M. Temporal and spatial analysis of COD concentration in East Dongting Lake by using of remotely sensed data. *Procedia Environ. Sci.* **2011**, *10*, 2703–2708. [CrossRef]
202. Bi, S.; Li, Y.; Wang, Q.; Lyu, H.; Liu, G.; Zheng, Z.; Du, C.; Mu, M.; Xu, J.; Lei, S.; et al. Inland water Atmospheric Correction based on Turbidity Classification using OLCI and SLSTR synergistic observations. *Remote Sens.* **2018**, *10*, 1002. [CrossRef]
203. Chavez, P.S. An improved dark-object subtraction technique for atmospheric scattering correction of multispectral data. *Remote Sens. Environ.* **1988**, *24*, 459–479. [CrossRef]
204. Adjovu, G.E. *Evaluating the Performance of A GIS-Based Tool for Delineating Swales Along Two Highways in Tennessee*; ProQuest LLC: Ann Arbor, MI, USA, 2020.
205. Banadkooki, F.B.; Ehteram, M.; Panahi, F.; Sammen, S.S.; Othman, F.B.; EL-Shafie, A. Estimation of total dissolved solids (TDS) using new hybrid machine learning models. *J. Hydrol.* **2020**, *587*, 124989. [CrossRef]
206. da Silva, M.G.; de Oliveira de Aguiar Netto, A.; de Jesus Neves, R.J.; Vasco, A.N.D.; Almeida, C.; Faccioli, G.G. Sensitivity Analysis and Calibration of Hydrological Modeling of the Watershed Northeast Brazil. *J. Environ. Prot.* **2015**, *06*, 837–850. [CrossRef]
207. Moriasi, D.N.; Arnold, J.G.; Van Liew, M.W.; Bingner, R.L.; Harmel, R.D.; Veith, T.L. Model Evaluation Guidelines for Systematic Quantification of Accuracy in Watershed Simulations. *Trans. ASABE* **2007**, *50*, 885–900. [CrossRef]
208. Sun, K.; Rajabtabar, M.; Samadi, S.; Rezaie-Balf, M.; Ghaemi, A.; Band, S.S.; Mosavi, A. An integrated machine learning, noise suppression, and population-based algorithm to improve total dissolved solids prediction. *Eng. Appl. Comput. Fluid Mech.* **2021**, *15*, 251–271. [CrossRef]
209. Kutser, T. Passive optical remote sensing of cyanobacteria and other intense phytoplankton blooms in coastal and inland waters. *Int. J. Remote Sens.* **2009**, *30*, 4401–4425. [CrossRef]
210. Li, Z.; Zhang, H.K.; Roy, D.P.; Yan, L.; Huang, H.; Li, J. Landsat 15-m Panchromatic-Assisted Downscaling (LPAD) of the 30-m reflective wavelength bands to Sentinel-2 20-m resolution. *Remote Sens.* **2017**, *9*, 755. [CrossRef]
211. USDA. *Resampling and Pansharping Using Raster Functions in ArcPro*; Forest Service, USDA: Washington, DC, USA, 2021; pp. 1–8.
212. Vanhellemont, Q.; Ruddick, K. Acolite for Sentinel-2: Aquatic applications of MSI imagery. *Eur. Symp. Agency* **2016**, *SP-740*, 9–13.
213. Li, J.; Chen, X.; Tian, L.; Huang, J.; Feng, L. Improved capabilities of the Chinese high-resolution remote sensing satellite GF-1 for monitoring suspended particulate matter (SPM) in inland waters: Radiometric and spatial considerations. *ISPRS J. Photogramm. Remote Sens.* **2015**, *106*, 145–156. [CrossRef]